nature communications

Article

https://doi.org/10.1038/s41467-024-54882-y

Phenazine biosynthesis-like domain-containing protein (PBLD) and Cedrelone promote antiviral immune response by activating NF-κB

Received: 15 March 2024

Accepted: 21 November 2024

Published online: 08 January 2025

Check for updates

Peili Hou[1,2,4], Hongchao Zhu[1,4], Fengyun Chu[1], Yan Gao[1], Xiaonan Sun[1], Fuzhen Zhang[2], Xiaomeng Wang[1], Yueyue Feng[1], Xingyu Li[1], Yu Liu[1], Jun Wang[1], Xiaoyun Wang[1], Daniel Chang He[3], Hongmei Wang[1,5] ✉ & Hongbin He[1,2,5] ✉

Phenazine biosynthesis-like domain-containing protein (PBLD) and Cedrelone have been identified as tumor suppressors. However, their roles in virus infection remain unclear. Here, we demonstrate that PBLD upregulates the type I interferon (IFN-I) response through activating NF-kappaB (NF-κB) signaling pathway to resist viral infection in cells and mice. Mechanistically, PBLD activates NF-κB signaling pathway during viral infection via blocking tripartite motif containing 21 (TRIM21)-mediated phosphorylated inhibitory kappa B kinase beta (IKKβ) degradation. Furthermore, we show Cedrelone inhibits viral replication by increasing the PBLD protein expression and subsequently activating NF-κB-mediated IFN-I response. Furthermore, the therapeutic potential of Cedrelone lies in its ability to enhance antiviral immunity in primary macrophages and to promote survival and reduce lung tissue damage in HSV-1-infected mice in a PBLD-dependent manner. Consequently, our findings provide a potential combination model that targets PBLD for Cedrelone antiviral drug therapy, potentially paving the way for the development of broad-spectrum antiviral agents.

Pandemic viral infectious diseases, with their increasing viral transmissibility and pathogenesis, have emerged as significant global challenges, posing threats not only to the well-being and lives of animals and humans, but also causing unprecedented casualties and economic burdens on society[1,2]. Consequently, combating viral infections has become a paramount global concern. The identification of pivotal host genes that affect viral replication will have profound implications for the development of novel broad-spectrum antiviral drugs, which represent a crucial and effective strategy in addressing sudden outbreaks of viral infectious diseases.

Type I interferon (IFN-I) signaling is essential for the innate immunity defense against viral infections[3]. The recognition of cytosolic viral nucleic acids, known as pathogen-associated molecular patterns (PAMPs), by pattern-recognition receptors (PRRs) such as RIG-I or cGAS initiates specific signaling pathways. These pathways activate IRF3, IRF7, and NF-κB, leading to the expression of IFN-I, interferon-stimulated genes (ISGs) and pro-inflammatory cytokines, which then restrict viral infection[4,5]. However, the mechanisms underlying the self-regulation of IFN-I signaling remain largely unknown. Therefore, the discovery of molecules that influence innate

[1]Ruminant Diseases Research Center, College of Life Sciences, Shandong Normal University, Jinan, Shandong, China. [2]Department of Preventive Veterinary Medicine, College of Veterinary Medicine, Shandong Agricultural University, Taian, Shandong, China. [3]The College of Arts and Sciences, University of North Carolina at Chapel Hill, Chapel Hill, NC, USA. [4]These authors contributed equally: Peili Hou, Hongchao Zhu. [5]These authors jointly supervised this work: Hongmei Wang, Hongbin He. ✉e-mail: hongmeiwang@sdnu.edu.cn; hongbinhe@sdnu.edu.cn

immune response would greatly aid in the development of effective antiviral treatments.

The nuclear factor kappa B (NF-κB) is an inducible and versatile transcription factor involved in various biological processes, such as immune responses, inflammatory responses, cellular differentiation, and apoptosis[6,7]. In mammals, NF-κB activation involves two well-characterized signaling pathways: the canonical and non-canonical pathways[8,9]. The canonical pathway facilitates the activation of NF-κB dimers composed of the p65, c-Rel, and p50 subunits. In resting cells, NF-κB dimers interact with inhibitory IκB proteins, which retain them in the cytoplasm. Upon stimulation, the activated IκB kinase (IKK) complex (IKKα/β/γ) phosphorylates IκBα (Ser32), leading to its rapid proteasome degradation. This degradation allows free NF-κB complexes to translocate to the nucleus, and activate the expression of hundreds of immunomodulatory proteins, pro-inflammatory cytokines, chemokines, and growth factors[10–12]. Viruses play a crucial role in modulating the NF-κB cascade and have developed various mechanisms to either activate or inhibit this pathway, thus promoting viral multiplication and the establishment of infection[13,14]. Furthermore, multiple viruses target the IKK complex, impairing host antiviral responses and enhancing viral infection[15–17].

Phenazine biosynthesis-like domain-containing protein (PBLD) is an isomerase protein that was initially identified as an interacting partner of mitogen-activated protein kinase activator with WD40 repeats (MAWD) through yeast two-hybrid technology[18]. PBLD is expressed in various tissues and represents the sole member of the phenazine biosynthesis-like protein family in the human genome. Crystal structures of human PBLD reveal characteristic satellite growth[19]. PBLD is primarily involved in tumor development, with studies demonstrating that its forced expression impacts multiple downstream genes associated with MAPK, NF-κB, EMT(Epithelial-Mesenchymal Transition), and angiogenesis signaling pathways[20–22]. Co-expression of PBLD and MAWD has been shown to suppress the phosphorylation and nuclear translocation of p-Smad3[23]. Moreover, PBLD overexpression in intestinal epithelial cells consistently inhibits TNF-α/interferon-γ-induced disruption of intestinal barrier and TNF-α-induced inflammatory responses[21]. However, the role of PBLD in viral infection remains unexplored.

Cedrelone is a highly oxygenated tetracyclic triterpene derivative known as a limonoid[24]. Previous studies have demonstrated that Cedrelone is capable of inhibiting colony formation, cell adhesion, migration, and invasion, while also acting as a potent inducer of apoptosis and causing cell cycle arrest[25]. Mounting evidence suggests that Cedrelone exhibits antitumor effects and significant cytotoxicity against various cancer cell lines, including HL-60, SMMC-7721, A549, MCF-7 and SW480[24,26]. Furthermore, Cedrelone possesses treated-hepatocellular carcinoma capabilities via targeted PBLD overexpression[27]. However, the role of Cedrelone in viral infection has remained ambiguous.

In this study, we demonstrate that PBLD and its activator, Cedrelone, potentiates cellular antiviral responses. Our results indicate that PBLD not only stimulates IFN-I production through NF-κB signaling pathway in vitro using cell lines but also in vivo using *Pbld*-deficient mice models. We reason that PBLD with a broad-spectrum antiviral activity against various viruses is likely to promotion of antiviral immunity response mechanism that is commonly used by multiple RNA and DNA virus, including vesicular stomatitis virus (VSV), Sendai virus (SeV), bovine ephemeral fever virus (BEFV), bovine parainfluenza virus 3 (BPIV3) and the herpesviruses (HSV-1). We further elucidate that PBLD activates the NF-κB signaling pathway through blocking the degradation of TRIM21 on phosphorylated IKKβ upon virus infection. More importantly, we discover that Cedrelone enhances the antiviral response depending on PBLD/NF-κB-mediated IFN-I signaling pathway. These findings uncover the biological function of PBLD and Cedrelone, which may contribute to the development of control strategies for the antiviral therapy.

Results

PBLD positively regulates the IFN-I immune response against BPIV3 or HSV-1 replication

Since PBLD is primarily associated with tumor suppression, its involvement in antiviral immunity has not been explored. We utilized BPIV3 and HSV-1 as viral models to evaluate the impact of PBLD on virus-induced IFN-I response. Firstly, we generated MDBK and HeLa cell lines with stable expression of Flag epitope-tagged PBLD (Supplementary Fig. 1a, b). Then the production of type I IFNs and ISGs in BPIV3 infected MDBK cell lines, and HSV-1 infected or poly(dA:dT) transfected HeLa cell lines were determined by RT-qPCR. The results revealed that the transcripts of IFNs and ISGs were increased in PBLD-overexpressing cell lines compared to the control cell lines (Fig. 1a, Supplementary Fig. 1c, d). Furthermore, a substantial upregulation of ISG proteins in HSV-1-infected or poly(dA:dT)-transfected PBLD overexpressed HeLa cells was observed (Fig. 1b, c), indicating that overexpression of PBLD promotes the IFN-I response upon viral infection.

Additionally, we generated PBLD knockout (KO) MDBK and HeLa cell lines using CRISPR-Cas9 gene-editing technology (Supplementary Fig. 1e, f). After MDBK cell lines infected with BPIV3 or HeLa cell lines infected with HSV-1 or treated with Poly(dA:dT) for indicated time, respectively, the transcripts of type I IFNs and ISGs were decreased in PBLD KO cell lines compared to control cell lines (Fig. 1d and Supplementary Fig. 1g, h). Moreover, knockout of PBLD expression resulted in a significant reduction in ISG protein levels after HSV-1 infection or Poly(dA:dT) transfection (Fig. 1e, f), suggesting that knockout of PBLD inhibits the IFN-I immune response upon viral infection.

To further verify the role of PBLD in the IFN-I immune response with a broad-spectrum, we subjected embryonic fibroblasts (MEFs) from WT (*Pbld*$^{+/+}$) and *Pbld* knockout (*Pbld*$^{-/-}$) mice to DNA (HSV-1) and RNA virus (BPIV3, VSV and SeV) as well as RNA virus mimic poly (I:C) and DNA virus mimic poly(dA:dT) transfection, respectively. Consistently, our data showed that *Pbld* deficiency in MEFs down-regulated the mRNA level of *Ifna4, Ifnb1, Isg15, Isg56,* and protein production of IFN-α and IFN-β upon viral infection, poly(I:C) or poly(dA:dT) stimulation (Supplementary Fig. 2a–d). Furthermore, PBLD could suppress different doses of VSV and HSV-1(0.1, 1 and 5 MOI)- induced IFN-I response in *Pbld*$^{-/-}$ MEFs compared to *Pbld*$^{+/+}$ MEFs (Supplementary Fig. 2e, f). These data together demonstrated that PBLD is involved in multiple virus-triggered IFN-I response.

To establish PBLD promoted IFN-I response with antiviral effect, the viral titers, viral gene and viral protein were determined in MDBK and HeLa cell lines with PBLD overexpression following BPIV3 and HSV-1 stimulation at different time periods. As shown in Fig. 1g, Supplementary Fig. 3a–d, the virus titers, viral genes and viral proteins of BPIV3 and HSV-1 in PBLD-Flag cell lines were lower than that of control cells over time. Conversely, knockout of PBLD had the opposite effect (Fig. 1h, Supplementary Fig. 3e–h). Similar results were also observed in BPIV3 and HSV-1 infected MEFs (Supplementary Fig. 3i–n). Taken together, our results demonstrate that PBLD positively regulates the type I IFN response and suppresses viral replication.

To further verify whether the viral inhibitory effect of PBLD was mediated by IFN-I, we used IFNAR1 neutralizing monoclonal antibody (Ab) to block the IFN-I signal pathway[28]. As shown in Supplementary Fig. 4a, b, treatment with the IFNAR antibody (Ab) significantly increased HSV-1 and BPIV3 infection as compared to the IgG isotype control. However, the inhibition of viral protein and titer of BPIV3 and HSV-1 by overexpression of PBLD was not significantly detected upon IFNAR1 Ab treatment compared with control cells (Supplementary Fig. 4a, b). Furthermore, the contributory effect on BPIV3 and HSV-1 replication by PBLD knockout was significantly weakened as compared with that of control cells after blocking the type I IFN response. And the titer and viral proteins of BPIV3 and HSV-1 in PBLD knock out cell lines and *Pbld*- deficient MEFs was not significantly changed after treatment

https://doi.org/10.1038/s41467-024-54882-y

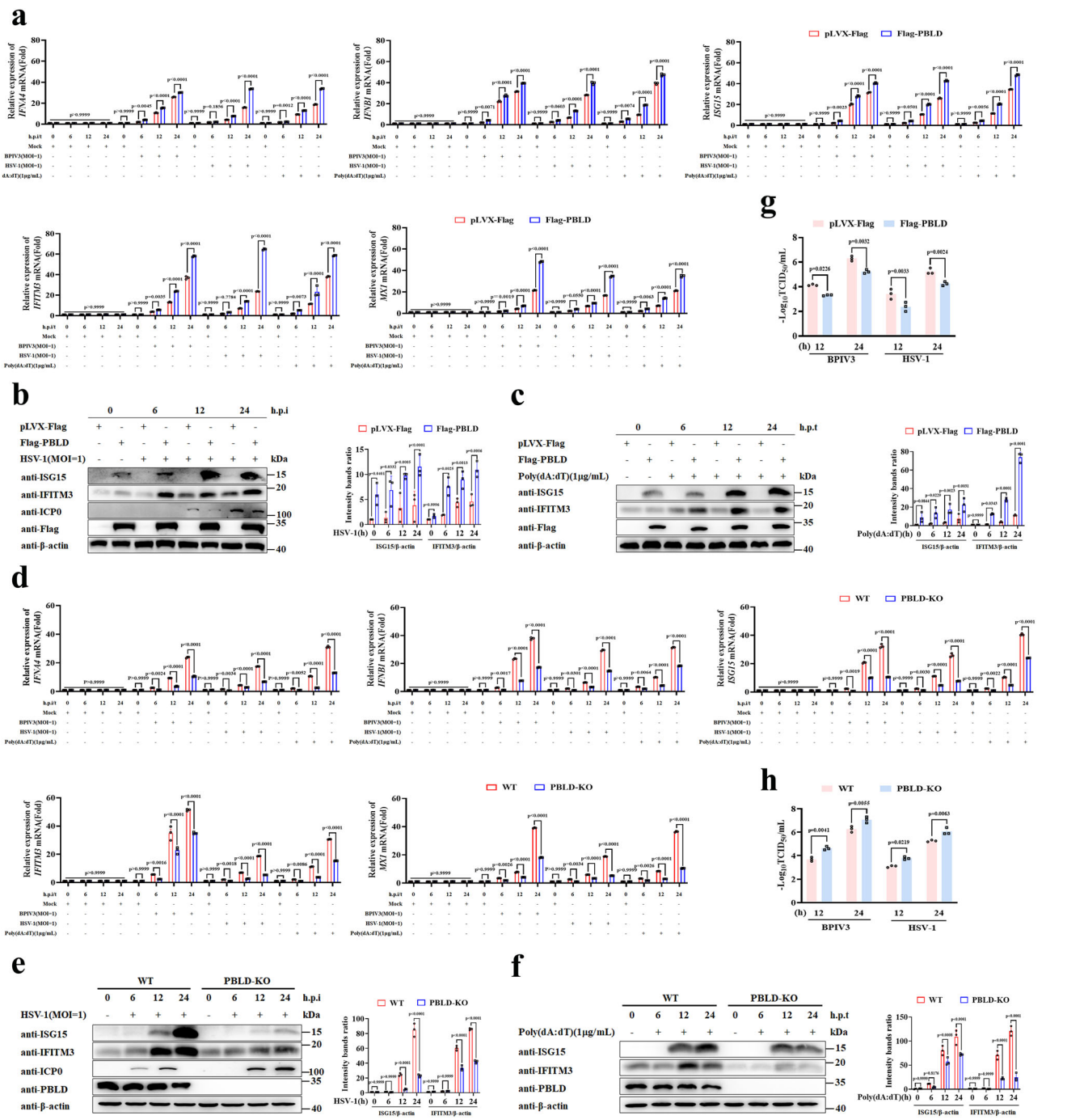

Fig. 1 | PBLD promotes virus infection-induced the IFN-I signaling pathway. **a** Real-time PCR analysis of the mRNA expression of IFNs and ISGs in BPIV3 (MOI = 1) infected PBLD-overexpression of MDBK cell lines (Flag-PBLD), and HSV-1 (MOI = 1) infected or poly(dA:dT) (1 μg/mL) transfected PBLD-overexpression of HeLa cell lines (Flag-PBLD) and corresponding control cell lines (pLVX-Flag) for the indicated time points. Western blotting analysis the ISG proteins expression in PBLD-overexpressing HeLa cell lines infected with HSV-1 (MOI = 1) (**b**) or transfected with poly(dA:dT) (1 μg/mL) (**c**) for the indicated time points. The bar chart indicates the ratios of ISG proteins band density to β-actin. **d** Real-time PCR analysis of the mRNA expression of IFNs and ISGs in PBLD knockout MDBK cell lines (PBLD-KO) or control cell lines (WT) in response to BPIV3 (MOI = 1) infection, and PBLD knockout HeLa cell lines with HSV-1 (MOI = 1) infection or poly(dA:dT) (1 μg/mL) transfection for the indicated time points. Western blotting analysis the ISG proteins expression in PBLD-knockdown HeLa cells infected with HSV-1 (MOI = 1) (**e**) or transfected with poly(dA:dT) (1 μg/mL) (**f**) for the indicated time points. The bar chart indicates the ratios of ISG proteins band density to β-actin. Virus titer detection determined by $TCID_{50}$ of BPIV3 in MDBK cell lines and HSV-1 in HeLa cell lines that stably over-expressed Flag-PBLD (**g**) or knockout of PBLD (**h**) after infection with BPIV3 or HSV −1 for the indicated time points, respectively; Data in (**a**, **d**, **g**, **h**) are presented as mean ± SD, two-way ANOVA; $n = 3$ biological independent experiments. Data in (**b**, **c**, **e**, **f**) are representative from three independent experiments. The gray intensity of the bands in (**b**, **c**, **e**, **f**) presented as mean ± SD from three independent experiments were analyzed using ImageJ software, two-way ANOVA. Source data are provided as a Source data file.

https://doi.org/10.1038/s41467-024-54882-y

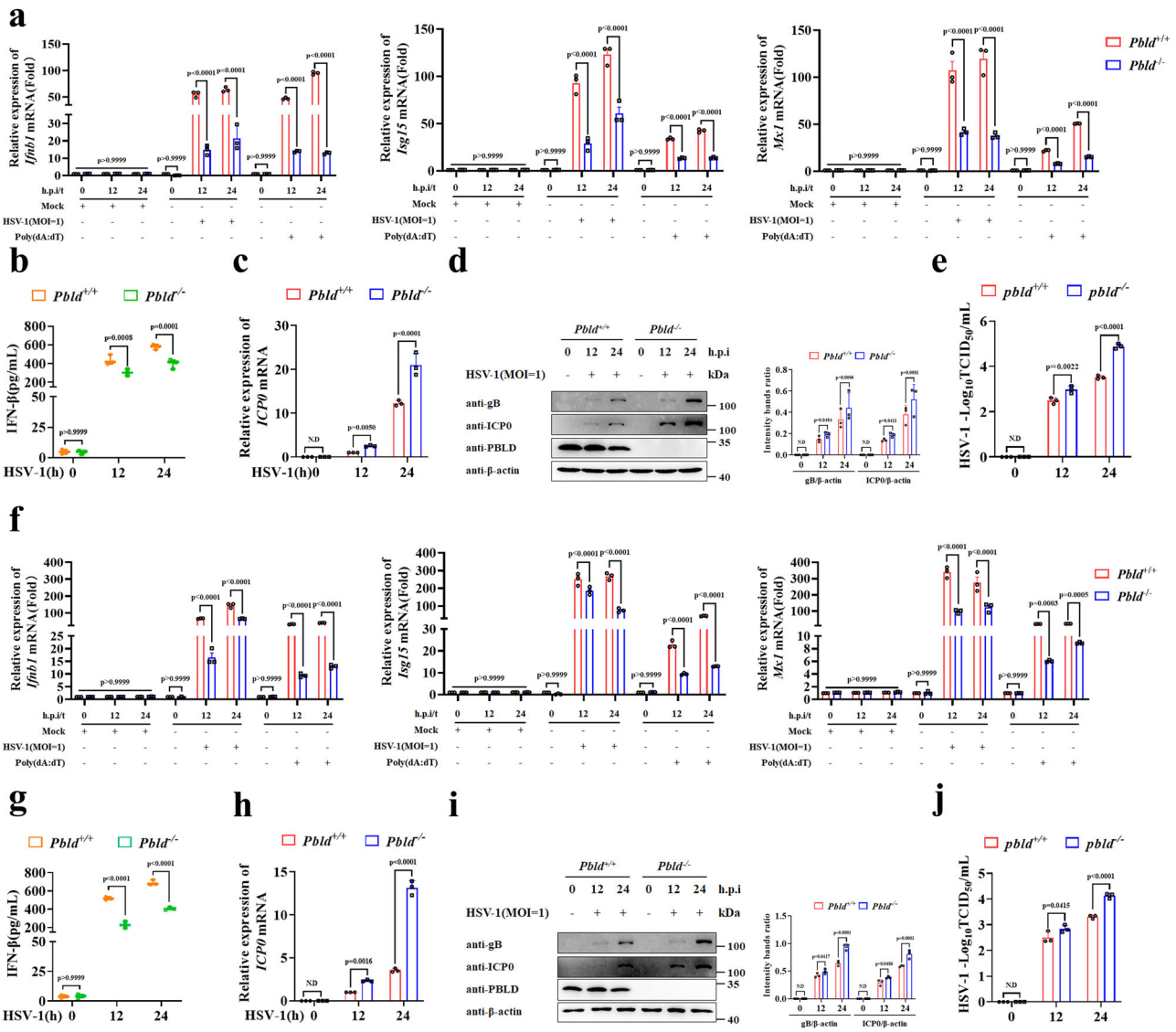

Fig. 2 | PBLD-deficient macrophage suppresses virus-induced the IFN-I response. a Real-time PCR analysis the mRNA levels of IFNs and ISGs in PMs from eight-week-old *Pbld*$^{+/+}$ and *Pbld*$^{-/-}$ mice infected with HSV-1 (MOI = 1), transfected with poly(dA:dT) (1 μg/mL) or without treatment (Mock) for indicated time points, respectively. **b** ELISA assay of IFN-β in supernatants of *Pbld*$^{+/+}$ and *Pbld*$^{-/-}$ PMs, infected with HSV-1 (MOI = 1) for indicated time points. Real-time PCR, Western blotting and viral proteins band density analysis of the viral gene (**c**), proteins expression and the ratios of viral protein band density to β-actin (**d**) in *Pbld*$^{+/+}$ and *Pbld*$^{-/-}$ PMs, infected with HSV-1 (MOI = 1) for indicated time points. **e** Virus titer detection determined by $TCID_{50}$ of HSV-1 in *Pbld*$^{+/+}$ and *Pbld*$^{-/-}$ PMs at indicated time points. **f** Real-time PCR analysis the mRNA levels of IFNs and ISGs in BMDMs obtained from eight-week-old *Pbld*$^{+/+}$ and *Pbld*$^{-/-}$ mice, and infected with HSV-1 (MOI = 1), transfected with poly(dA:dT) (1 μg/mL) or without treatment (Mock) for indicated time points, respectively. **g** ELISA assay of IFN-β in supernatants of *Pbld*$^{+/+}$ and *Pbld*$^{-/-}$ BMDMs infected with HSV-1 (MOI = 1) for indicated time points. Real-time PCR, Western blotting and viral proteins band density analysis of the viral gene (**h**), proteins expression and the ratios of viral protein band density to β-actin (**i**) in HSV-1 (MOI = 1)-infected *Pbld*$^{+/+}$ and *Pbld*$^{-/-}$ BMDMs for indicated time points. **j** Virus titer detection determined by $TCID_{50}$ in *Pbld*$^{+/+}$ and *Pbld*$^{-/-}$ BMDMs infected with HSV-1 (MOI = 1) for indicated time points. N.D Not detected. Data in (**a**–**c**, **e**–**h**, **j**) are presented as mean ± SD, two-way ANOVA; $n = 3$ biological independent experiments. Data in (**d**, **i**) are representative from three independent experiments. The gray intensity of the bands in (**d**, **i**) presented as mean ± SD from three independent experiments were analyzed using ImageJ software; two-way ANOVA. Source data are provided as a Source data file.

with IFNAR1 Ab compared to the IgG isotype control (Supplementary Fig. 4c–f). Collectively, our results indicate that the inhibition of BPIV3 or HSV-1 infection by PBLD is dependent on IFN-I response.

Pbld deficiency in primary macrophages inhibits the antiviral immunity response

To further investigate the impact of PBLD on the IFN-I response, we extended our study to peritoneal macrophages (PMs), and bone-marrow-derived macrophages (BMDMs) derived from *Pbld*$^{+/+}$ and *Pbld*$^{-/-}$ mice. Accordingly, reduced IFN and ISGs mRNA and IFN-β protein expression in PMs with *Pbld* deficiency were observed in response to HSV-1 infection or poly(dA:dT) transfection (Fig. 2a, b). Moreover, *Pbld* deficiency in PMs markedly increased the *ICP0* mRNA, gB and ICP0 protein levels of HSV-1 as well as virus titer of HSV-1 (Fig. 2c–e). Similar results were also observed in *Pbld*-deficient BMDMs (Fig. 2f–j). Collectively, these results suggest that PBLD in macrophages functions as a positive regulator of antiviral IFN-I response.

PBLD promotes the antiviral IFN-I response by activating NF-κB signaling pathway

A previous study has shown a direct connection between PBLD and NF-κB signaling in intestinal barrier functional model[21]. Therefore, we

https://doi.org/10.1038/s41467-024-54882-y

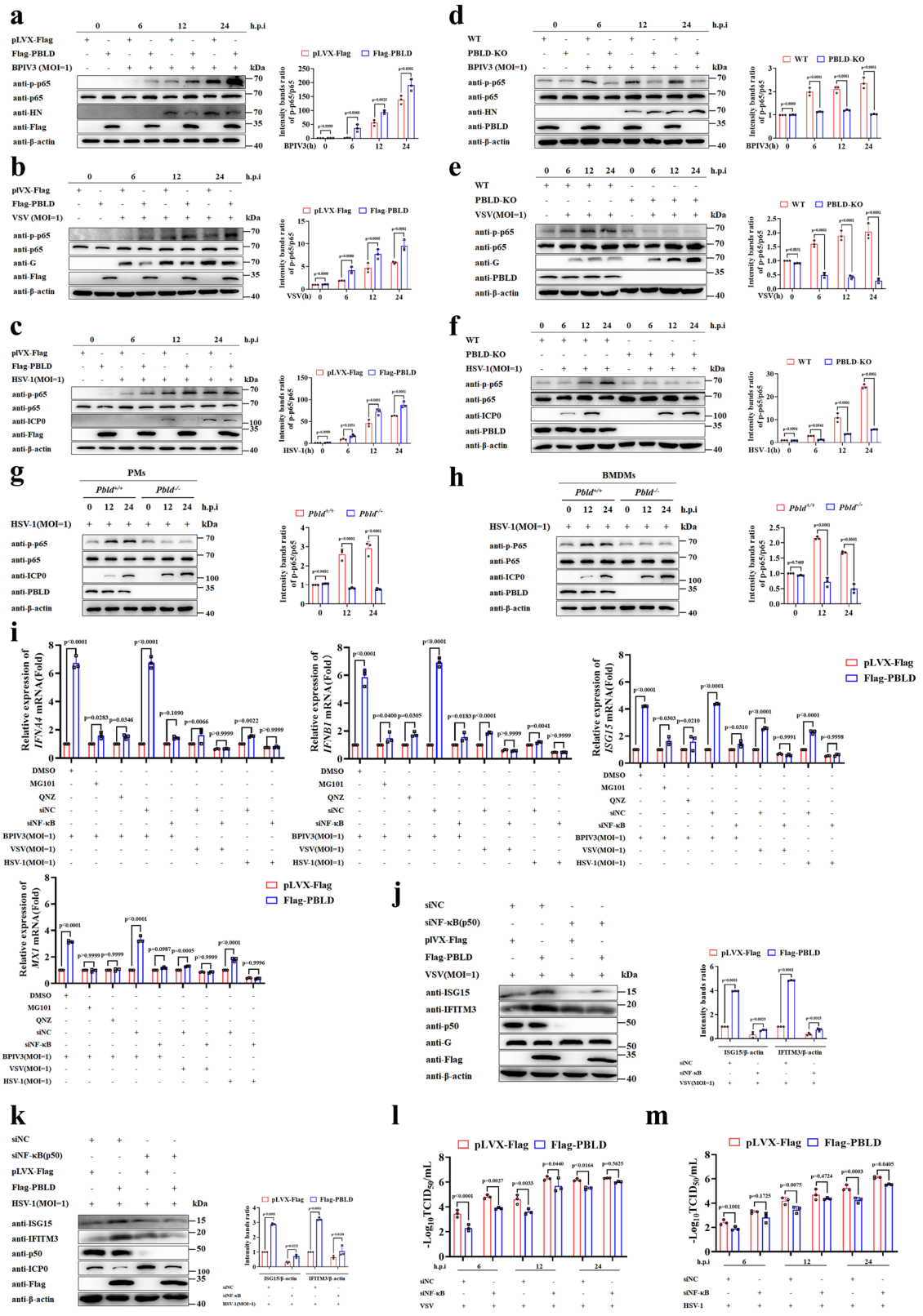

investigated whether PBLD promotes the IFN-I response through the NF-κB signaling pathway. As shown in Fig. 3a–c, an up-regulation of p-p65 protein level upon overexpression of PBLD after infection with BPIV3, VSV or HSV-1 was observed. On the contrary, knockout of PBLD had the opposite effect (Fig. 3d–f). Consistently, *Pbld* deficiency in MEFs significantly down-regulated the expression of p-p65 protein level in response to BPIV3, VSV, SeV, and HSV-1 infection (Supplementary Fig. 5a–d). Similar results were also observed in HSV-1 infected *Pbld*-deficient PMs and BMDMs (Fig. 3g, h). These findings strongly suggest that PBLD activates NF-κB signaling pathway during viral infection.

To investigate the roles of NF-κB in PBLD mediated IFN-I signaling pathway, we used two pharmacological inhibitors of NF-κB, MG-101 and QNZ. The optimal concentrations of MG-101 (20 μM) and QNZ

Fig. 3 | PBLD positively regulates the IFN-I response via activating NF-κB pathway. Western blotting analysis of the indicated protein expression in BPIV3 (MOI = 1) infected control cells (pLVX-Flag), PBLD-overexpressing (Flag-PBLD) MDBK cell lines (**a**), or Flag-PBLD-expressing HeLa cell lines upon VSV (MOI = 1) (**b**) or HSV-1 (MOI = 1) infection (**c**) for the indicated time points. Western blotting analysis of the indicated protein expression in BPIV3 (MOI = 1) infected with control cells (WT), PBLD knockout (PBLD-KO) (**d**) MDBK cell lines, or HeLa cell lines upon VSV (MOI = 1) (**e**) or HSV-1 (MOI = 1) infection (**f**) for the indicated time points. Western blotting analysis the indicated protein expression in *Pbld*$^{+/+}$ and *Pbld*$^{-/-}$ PMs (**g**) and BMDMs (**h**) upon HSV-1 (MOI = 1) infection for the indicated time points. **i** Real-time PCR analysis the mRNA expression of IFNs and ISGs in PBLD-overexpressing HeLa cells treated with DMSO, MG101 (20 μM) or QNZ (10 μM) or transfected with siNF-κB (10 nM) or siNC, and then infected with BPIV3 (MOI = 1), VSV (MOI = 1) or HSV-1 (MOI = 1), respectively for 24 h. Western blotting analysis the indicated protein expression in PBLD-overexpressing HeLa cells upon transfected with siNF-κB (10 nM) or siNC, and infected with VSV (MOI = 1) (**j**) and HSV-1 (MOI = 1) (**k**) for 24 h. Virus titer of VSV (**l**) or HSV-1 (**m**) detection determined by $TCID_{50}$ in stably overexpressed Flag-PBLD HeLa cell lines or control cells (pLVX-Flag) that were transfected with siNF-κB or siNC in response to VSV or HSV-1 for indicated time points. Data in (**a**–**h**, **j**, **k**) are representative from three independent experiments. The bar chart in (**a**–**h**, **j**, **k**) indicates the ratios of p-p65 band density to p65. The gray intensity of the bands presented as mean ± SD from three independent experiments were analyzed using ImageJ software, two-way ANOVA; Data in (**i**, **l**, **m**) are presented as mean ± SD, two-way ANOVA; $n = 3$ biological independent experiments. Source data are provided as a Source data file.

(10 μM) were determined through cell viability assays and western blot analyses (Supplementary Fig. 5e–h). Subsequently, HeLa cells and MDBK cells treated with MG-101 or QNZ exhibited reduced expression of IFNs and ISGs compared to those treated with DMSO in the content of BPIV3 and BEFV infection, respectively (Fig. 3i, Supplementary Fig. 5i). Consistently, there was no significant difference on the transcripts of *IFNA4, IFNB1, ISG15, MxX1, IL-6, and TNFA* in PBLD overexpression HeLa cells compared to control group after silencing NF-κB upon BPIV3, VSV, or HSV-1 infection (Fig. 3i, Supplementary Fig. 5j, k). Similar results were obtained in BEFV infected MDBK cells, HeLa cells transfected with Poly(I:C) and Poly(dA:dT) with PBLD overexpression or VSV and HSV-1 infected *Pbld* deficient MEFs when NF-κB was knocked down (Supplementary Fig. 5l–p). Furthermore, the ISGs protein induced by PBLD were substantially reduced after NF-κB knockdown upon VSV or HSV-1 infection (Fig. 3j, k). Notably, compared to control cells, overexpressing PBLD in HeLa cells or *Pbld* deficiency in MEFs suppressed or increased virus titers, but this effect was attenuated when NF-κB was knocked down in response to VSV and HSV-1 (Fig. 3l, m, Supplementary Fig. 5q), indicating that PBLD inhibits viral replication through the NF-κB signaling pathway. All in all, these data suggest that PBLD promotes the antiviral type I IFN response by activating NF-κB signaling pathway.

PBLD activates the NF-κB signaling pathway during viral infection via blocking the degradation of TRIM21 on phosphorylated IKKβ

Although recent study have reported that PBLD in intestinal epithelial cells (IECs) binding to IKKs can inhibit NF-κB activation in dextran sulfate sodium (DSS)-induced colitis[21], our data showed that PBLD in HeLa had no effect on NF-κB activation for a kinetic time point without virus infection (Supplementary Fig. 6a, b). Furthermore, PBLD was able to bind to IKKα and IKKβ in the mock infection group, however, this interaction was attenuated upon BPIV3 and HSV-1 infection (Fig. 4a, b, Supplementary Fig. 6c, d). Subsequently, the expression of p-p65, p-IκBα and p-IKK was increased in HeLa cells overexpressing PBLD versus vector control cells (Fig. 4c, Supplementary Fig. 6e, f). Conversely, knockout of PBLD had the opposite effects (Fig. 4d. Supplementary Fig. 6g, h), suggesting that the binding of PBLD to IKKα/β does not serve as a critical determinant for the formation of the IKKs complex.

To explore the specific mechanism by which PBLD activates NF-κB after viral infection, we performed immunoprecipitation (IP) combined with mass spectrometry (MS) analysis in BPIV3-infected PBLD-Flag expressed HeLa cells to identify which proteins were associated with PBLD (Fig. 4e). Among those candidate proteins, the tripartite motif containing 21 (TRIM21) is a negative regulator of NF-κB signaling pathway via autophagic degradation of phosphorylated IKKβ depending on its RING domain[29,30]. This indicates that TRIM21 might mediate PBLD activated NF-κB through suppression of the IKK complex activation, especially IKKβ phosphorylation. As expected, we found that PBLD was associated with TRIM21 in BPIV3 infected cells but not in mock infection (Fig. 4f, Supplementary Fig. 6i). This interaction was dependent on RING domain of TRIM21 (Fig. 4g). Consistent with previous reports, overexpression or silencing of TRIM21 during viral infection inhibited or elicited the activity of p-IKKβ (Supplementary Fig. 6j, k). And the inhibition of p-IKKβ activity by TRIM21 was dependent on its IRNG domain and occurred through autophagic degradation, as demonstrate by restoration of p-IKKβ expression after CQ treatment but not MG132 (Supplementary Fig. 6l, m). Furthermore, we found that TRIM21 interacted with p-IKKβ after viral infection, and upon overexpression of PBLD, TRIM21 interacting with p-IKKβ was attenuated (Fig. 4h, i). In contrast, knockout of PBLD had the opposite effect (Supplementary Fig. 6n, o), suggesting PBLD blocked the interaction of TRIM21 on p-IKKβ during viral infection. Moreover, overexpression of PBLD suppressed the ability of TRIM21 to inhibit p-IKKβ and p-p65 compared with control group (Fig. 4j), while overexpression of PBLD exhibited a slight promotional effect on p-IKKβ with TRIM21 knockdown compared with control group (Fig. 4k), suggesting that PBLD blocks the degradation of TRIM21 on p-IKKβ, and promotes NF-κB signaling pathway during viral infection.

More importantly, the effect of PBLD on the IFN-I response and viral replication with overexpressing/knocking down TRIM21 during viral infection were measured. These results demonstrated that overexpression of TRIM21 suppressed IFNs, ISGs, compared to vector control, whereas the inhibitory effect by overexpression of TRIM21 on the IFNs and ISGs expression was attenuated upon overexpression of PBLD (Fig. 4l). Accordingly, overexpression of TRIM21 increased the titer of BPIV3 compared with vector control, whereas the contributory effect of TRIM21 on viral replication was weaken in the presence of PBLD compared with control group (Fig. 4m). In contrast, knocking down TRIM21 resulted in increased IFNs, ISGs, and decreased viral titer compared to scrambled control. However, under the condition of TRIM21 knockdown, overexpression of PBLD slightly increased IFNs, ISGs, and slightly decreased viral titer compared to vector control (Fig. 4n, o). In summary, these data suggest that PBLD interacts with TRIM21 during viral infection, thereby blocking the degradation of TRIM21 on p-IKKβ, enhancing IKK kinase complex activity, and ultimately promoting the NF-κB/IFN-I activation and suppressing viral replication (Fig. 4p).

Pbld-deficient mice exhibit more susceptibility to HSV-1 infection

Next, we investigated the role of PBLD in mice against HSV-1infection (Fig. 5a). As shown in Fig. 5b, c, the *Pbld*$^{-/-}$ mice presented a stronger weight loss to HSV-1 infection, and their mortality rate was significantly higher compared to the wild type (WT) littermates. In addition, the transcriptional levels of *Ifnb1*, *Isg15*, and *Mx1* in the liver, lung, and spleen (Fig. 5d–f), and the production of IFN-α and IFN-β in the serum was reduced in *Pbld*$^{-/-}$ mice compared to the control group after HSV-1 infection (Supplementary Fig. 7a, Fig. 5g). Accordingly, *Pbld* deficiency led to increased expression of HSV-1 *gB* and *ICPO* genes in the liver, lung, and spleen (Fig. 5h–j). As shown by hematoxylin

https://doi.org/10.1038/s41467-024-54882-y

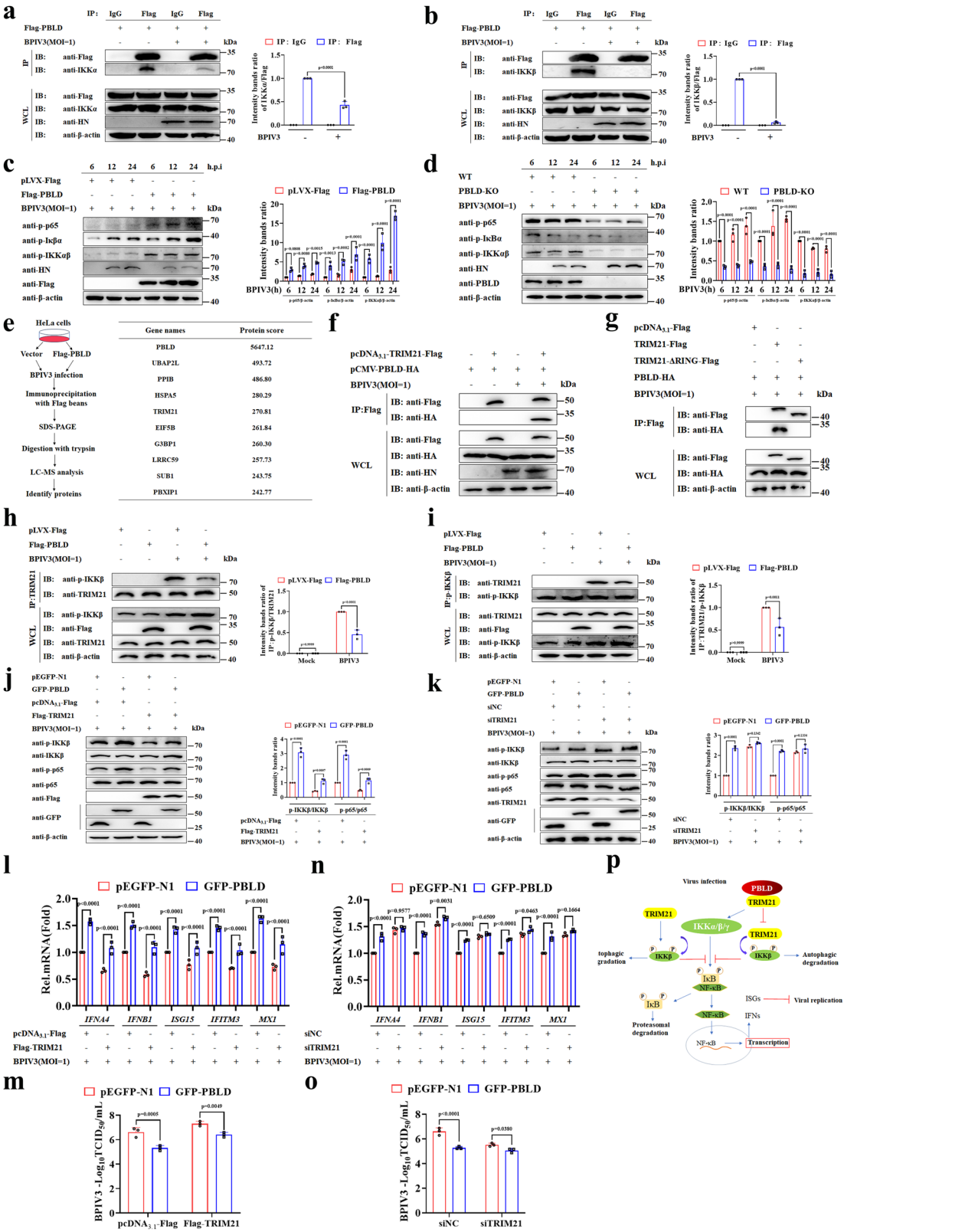

and eosin staining, the severity of pulmonary inflammation and lung lesions was significantly aggravated in *Pbld*$^{-/-}$ mice compared to WT mice at 2 dpi (Fig. 5k). Furthermore, consistent with the decreased levels of IFN and ISGs, the expression of p-p65 was significantly reduced in the liver, lung, and spleen (Fig. 5l–n). Thus, these data demonstrate that *Pbld* in mice is an important host factor in antiviral immune responses.

Finally, we addressed whether virus-induced IFN-I plays a critical role in HSV-1 infection in vivo. Consistently, *Pbld*$^{-/-}$ mice had decreased survival compared to the wild-type mice after HSV-1 infection in the absence of the antibody. However, blocking of type I IFN receptor in vivo significantly attenuated the decreased survival of mice by *Pbld* deficiency compared to wild type mice (Supplementary Fig. 7b). Correspondingly, there was no significant difference in the expression of

https://doi.org/10.1038/s41467-024-54882-y

Fig. 4 | PBLD activates NF-κB signaling pathway through binding to TRIM21 and blocking the degradation of TRIM21 on phosphorylated IKKβ during viral infection. The association of PBLD and IKKα (**a**) or IKKβ (**b**) was analyzed by Co-IP assay in the absence or presence of BPIV3 (MOI = 1) infection. Western blotting analysis of the indicated proteins expression in Flag-PBLD expressed (**c**) or PBLD-KO (**d**) HeLa cell lines upon BPIV3 infection for the indicated duration. **e** Scheme of the method for PBLD binding proteins and then identified by mass spectrometry in PBLD-overexpression (Flag-PBLD) HeLa cell lines and control cell lines (Vector) infected with BPIV3 (MOI = 1) for 12 h. The interaction between PBLD and TRIM21(**f**) or TRIM21-△RING-Flag (**g**) was analyzed by Co-IP assay. **h**, **i** TRIM21 co-immunoprecipitated (IP) with p-IKKβ in PBLD-overexpressing (Flag-PBLD) cells or control cells (pLVX-Flag) without (Mock) or with BPIV3 infection for 12 h. Western blotting analysis the indicated protein expression in HeLa cells transfected with GFP-PBLD-Flag, pEGFP-N1 vector control after overexpression of TRIM21 (**j**), knockdown of TRIM21 (**k**) with transfection of siTRIM21 or control siRNA (siNC), upon BPIV3 infection for 12 h. Real-time PCR analysis the mRNA expression of IFNs and ISGs (**l**, **n**) and virus titer determined by $TCID_{50}$ of BPIV3 (**m**, **o**) in HeLa cells transfected with GFP-PBLD-Flag, pEGFP-N1 vector control after overexpression of TRIM21 or vector control, transfection with siTRIM21(10 nM) or siNC, respectively, and infected with BPIV3. **p** Model depicting PBLD activated NF-κB signaling pathway. IP immunoprecipi tation, WCL whole cell lysates. Data in (**a**–**d**, **f**–**k**) are representative from three independent experiments. The gray intensity of the bands in (**a**–**d**, **h**–**k**) presented as mean ± SD from three independent experiments were analyzed using ImageJ software. Statistical analysis of intensity quantitation was performed by two-tailed Student's t-test in (**a**, **b**) and two-way ANOVA in (**c**, **d**, **h**–**k**). Data in (**l**–**o**) are presented as mean ± SD, $n = 3$ biological independent experiments; two-way ANOVA. Source data are provided as a Source data file.

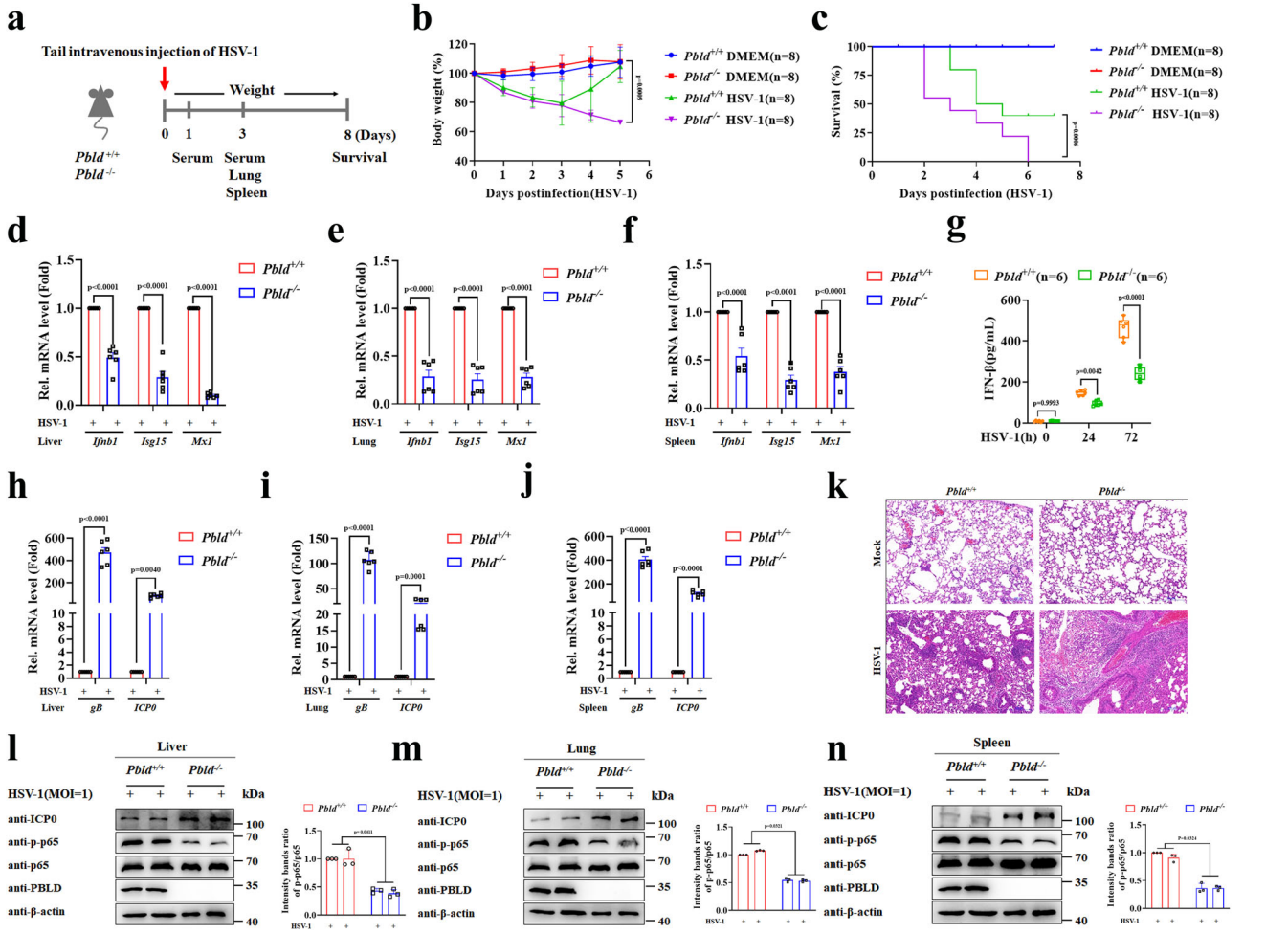

Fig. 5 | *Pbld*-deficient mice were susceptible to HSV-1 infection. a Schematic of eight-week-old *Pbld*$^{+/+}$ and *Pbld*$^{-/-}$ mice were injected with HSV-1 (2×10^7 PFU/mouse) via tail intravenous injection, respectively. **b** Body weight was recorded following HSV-1 infection in the first 5 days ($n = 8$ for each group). **c** Survival was estimated by the Kaplan–Meier method and compared by two-side log-rank test ($n = 8$ for each group). Real-time PCR analysis the mRNA levels of *Ifnb1*, *Isg15*, and *Mx1* in liver (**d**), lung (**e**) and spleen (**f**) from *Pbld*$^{+/+}$ and *Pbld*$^{-/-}$ mice ($n = 6$ for each group) with HSV-1 infection, respectively. **g** The IFN-β protein expression was detected by ELISA in the serum from *Pbld*$^{+/+}$ and *Pbld*$^{-/-}$ mice ($n = 6$ for each group) with HSV-1 infection for the indicated time points. Real-time PCR analysis the mRNA levels of HSV-1 *gB* and *ICP0* in liver (**h**), lung (**i**) and spleen (**j**), respectively. **k** Hematoxylin and eosin stained images of lung from *Pbld*$^{+/+}$ and *Pbld*$^{-/-}$ mice with or without HSV-1 infection, respectively. Scale bars, 100 μm. Western blotting analysis of the indicated proteins in liver (**l**), lung (**m**) and spleen (**n**) from *Pbld*$^{+/+}$ and *Pbld*$^{-/-}$ mice with HSV-1 infection, respectively. Data in (**b**, **d**–**j**) are presented as mean ± SD, $n = 8$ for (**b**), $n = 6$ for (**d**–**j**) biologically independent experiments. Statistical significance was determined using two-tailed Student's *t* tests in (**b**) or two-way ANOVA in (**d**–**j**); the box plots in (**g**) are defined in terms of minima, maxima, center, bounds of box and whiskers and percentile. Data in (**k**–**n**) are representative from three independent experiments. The gray intensity of the bands in data (**l**–**n**) presented as mean ± SD, $n = 3$ biologically independent samples, were analyzed using ImageJ software. Statistical analysis of intensity quantitation was performed by two-tailed Student's t-test. Source data are provided as a Source data file.

https://doi.org/10.1038/s41467-024-54882-y

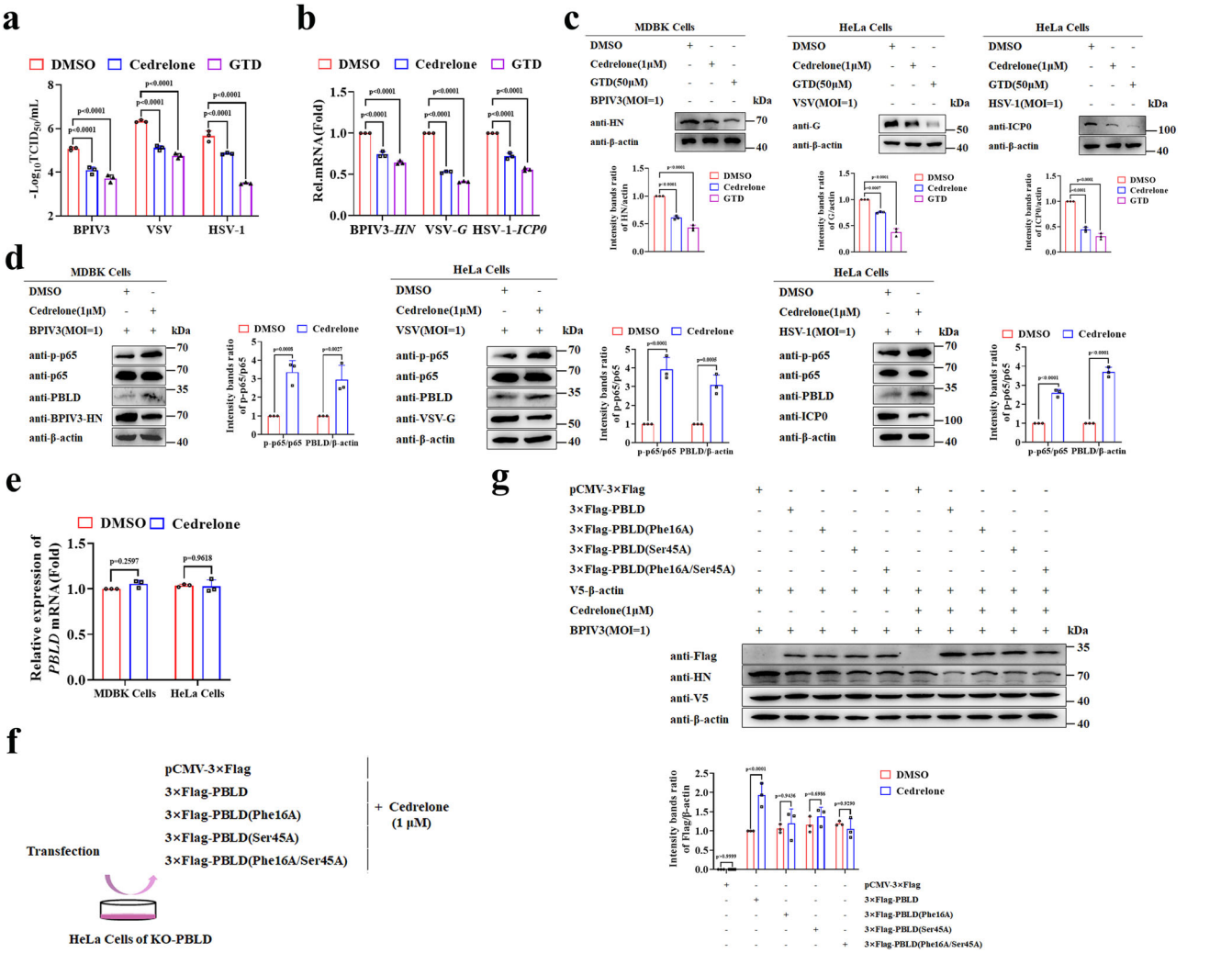

Fig. 6 | Cedrelone upregulates PBLD expression, activates NF-κB, and suppresses viral replication. a Virus titer detection of BPIV3, VSV, and HSV-1 determined by $TCID_{50}$ after challenge with DMSO (vehicle control) and Cedrelone (1 μM), and Gastrodin[61] (GTD, 50 μM) serves as a positive control. **b**, **c** Real-time PCR and Western blotting analysis of the viral gene and protein expression in BPIV3 infected MDBK cells and VSV or HSV-1 infected HeLa cells after challenge with DMSO, Cedrelone (1 μM) and GTD (50 μM). **d** Western blotting analysis of the indicated proteins expression in BPIV3 infected MDBK cells and VSV or HSV-1 infected HeLa cells after challenge with DMSO and Cedrelone (1 μM). **e** Real-time PCR analysis the mRNA levels of *PBLD* expression in MDBK and HeLa cells after challenge with DMSO and Cedrelone (1 μM). Schematic of the workflow of experiments (**f**), and western blotting analysis of the indicated proteins (**g**), and V5-β-actin as a control for transfection efficiency. Data in (**a**, **b**, **e**) are presented as mean ± SD, two-way ANOVA; $n = 3$ biological independent experiments. Data in (**c**, **d**, **g**) are representative from three independent experiments. The gray intensity of the bands in data (**c**, **d**, **g**) presented as mean ± SD from three independent experiments were analyzed using ImageJ software. Statistical analysis of intensity quantitation in (**c**, **d**, **g**) was performed by two-way ANOVA. Source data are provided as a Source data file.

ISGs and the titer of HSV-1 in lung tissue between *Pbld*$^{-/-}$ mice and wild type mice after blocking of the type I IFN receptors in vivo (Supplementary Fig. 7c, d). Collectively, PBLD mainly restricts virus replication via the type I IFN response.

Cedrelone has antiviral activity and upregulates the PBLD protein expression

Cedrelone is a chemical activator of PBLD that has demonstrated capabilities in treating HCC through targeted PBLD overexpression[27]. To investigate its role in viral infection, the CC_{50} and IC_{50} of Cedrelone against BPIV3, VSV, and HSV-1 in indicated cells were investigated by observing reduced cytopathic effect. All of the SI values were greater than 1 (Supplementary Table 3), indicating the potential of Cedrelone against various viruses. Subsequently, we found that Cedrelone (1 μM) markedly reduced virus titers of BPIV3, VSV, and HSV-1, and decreased the expression of viral genes and proteins compared to the DMSO control group (Fig. 6a–c). More importantly, we discovered that Cedrelone upregulated the protein expression of PBLD, activated the NF-κB pathway during BPIV3, VSV, and HSV-1 infection (Fig. 6d). Furthermore, we assessed the antiviral function of Cedrelone in MEFs. The different doses of Cedrelone (0.5 μM and 1 μM) suppressed VSV or HSV-1(1MOI) titers at 12 and 24 h but not 6 h (Supplementary Fig. 8a, b). Correspondingly, the VSV-*G* and HSV-1 *ICP0* mRNA and protein levels were also reduced under the same conditions (Supplementary Fig. 8c–f). Moreover, we found that Cedrelone treatment at concentrations of (0.5 μM and 1 μM) reduced viral titers, viral mRNA and proteins of VSV and HSV-1 under different amounts of particles (0.1 and 1 MOI), however, Cedrelone at concentrations of 1 μM instead of 0.5 μM treatment could inhibit 5 MOI VSV or HSV-1 replication (Supplementary Fig. 8g–l). Additionally, the Cedrelone compound did not affect the *PBLD* mRNA expression in MDBK cells and HeLa cells (Fig. 6e). These data consistently suggest that Cedrelone has the capacity to upregulate PBLD and NF-κB signaling pathway and attenuate virus productive infection in multiple cells.

To investigate the underlying mechanisms of how Cedrelone functions on PBLD, a molecular docking study between PBLD and Cedrelone with the binding site of PBLD, specifically Ser 45 and Phe 16 was predicted with AutoDock Vina software and visualized by PyMOL software. Subsequently, single and double mutants of PBLD were successfully constructed (PBLD(Phe16A), PBLD(Ser45A), PBLD(Phe16A/Ser45A)). Then wild type or mutants of PBLD were introduced into PBLD knockout cell lines together with Cedrelone treatment, respectively (Fig. 6f). As shown in Fig. 6g, treatment with Cedrelone resulted in an increased expression of wild-type PBLD, but not the single mutant at the Phe16 or Ser45 site and the double mutants at Phe16/Ser45 of PBLD compared to treatment with DMSO, indicating that the residue Phe16 and Ser45 of PBLD are key sites for Cedrelone to upregulate PBLD expression.

Cedrelone enhances the antiviral IFN-I response in a PBLD-dependent manner

Given that PBLD inhibits viral replication by activating the IFN-I signaling pathway, we hypothesize that Cedrelone also inhibits viral replication by promoting the activation of the IFN-I signaling pathway. As expected, Cedrelone treatment increased the expression of INFs or ISGs in response to BPIV3, VSV, or HSV-1 infection, respectively, whereas it had no effect in PBLD knockout cell lines (Fig. 7a–c, Supplementary Fig. 9a–d). Correspondingly, we observed a reduction in viral genes of BPIV3 (*HN*), VSV (*G*), and HSV-1 (*ICP0*) upon treatment with Cedrelone at a concentration of 1 μM in wild type cells, but not in the PBLD knockout cells (Fig. 7d–f), demonstrating that Cedrelone enhances the antiviral immune response in a PBLD-dependent manner. Furthermore, whether Cedrelone exerts antiviral IFN-I effect depending on the residue Phe16 and Ser 45 of PBLD was measured after introducing the wild type or mutants of PBLD into PBLD knockout cell lines. These experiments demonstrated that the single mutants of PBLD Ser 45 or Phe 16, especially Phe 16, and the double mutant of PBLD significantly weakened the upregulation of IFNs and ISGs by Cedrelone compared to transfection with wild-type PBLD during BPIV3, VSV or HSV-1 infection (Fig. 7g). Additionally, compared to transfection with wild-type PBLD, Cedrelone weakened its inhibitory effect on viral gene expression of BPIV3 (*HN*), VSV (*G*), and HSV-1 (*ICP0*) after expressing single or double mutants of PBLD Ser 45 and Phe 16 (Fig. 7h). Overall, Cedrelone specifically targets Phe 16 and Ser 45 of PBLD and exerts an antiviral effect.

Cedrelone promotes antiviral immunity in primary macrophages and attenuates HSV-1 infection in mice depending on PBLD

Next, the effect of Cedrelone on antiviral immunity in primary macrophages in response to HSV-1 infection was further investigated. As shown in Fig. 8a, b, an increased IFNs and ISGs were observed in the Cedrelone-treated PMs and BMDMs from wild mice but not in *Pbld* knockout mice. Additionally, Cedrelone treatment exhibited a reduced the mRNA levels of HSV-1 *ICP0* in both $Pbld^{+/+}$ PMs and BMDMs as compared to DMSO treatment, however, this phenomenon was not observed in $Pbld^{-/-}$ PMs and BMDMs (Fig. 8c, d). These data indicate that Cedrelone can promote the antiviral immunity response in primary macrophages depending on PBLD.

To confirm whether Cedrelone inhibits virus infection in vivo, $Pbld^{+/+}$ and $Pbld^{-/-}$ mice were challenged with HSV-1 or mock inoculated, and subsequent administration of Cedrelone or DMSO, respectively. As shown in Fig. 8e, compared to DMSO treatment, Cedrelone administration exhibited the higher survival rate of wild mice but not $Pbld^{-/-}$ mice that of infected with HSV-1. Correspondingly, Cedrelone administration showed a significant increase of the IFN-I response, and markedly upregulated the expression of *Pbld* and phosphorylated p65 but reduced HSV-1 ICP0 expression and viral titer compared to DMSO control in lung of wild mice instead of $Pbld^{-/-}$ mice (Fig. 8f–i). Additionally, the changes in pathological tissue analyzed by H&E showed that the tissue of lung exhibiting alveolar wall thickening, edema, stromal hyperplasia, compared with the blank control group, while Cedrelone supplementation reduced pathological damage to the lung. However, there was no significant difference in the pathological lesion of lung from $Pbld^{-/-}$ mice between Cedrelone treatment and control group (Fig. 8j). Taken together, these data demonstrate that Cedrelone has an inhibitory effect on HSV-1 infection in mice depending on PBLD.

Discussion

In this study, we discover that PBLD is an important positive regulator of IFN-I through activated NF-κB signaling pathway during virus infection. These findings were validated in different cells in vitro including passaged cells, primary cells and macrophages, as well as in vivo mouse models. However, concerning whether PBLD could influence the cell cycle and apoptosis in HeLa cells, flow cytometry analysis showed that PBLD slightly triggered G2/M cell cycle arrest, but not affected apoptosis in the absence of viral infection (Supplementary Figs. 10a–d, 11a–d). In contrast, after viral infection, PBLD could induce apoptosis (Supplementary Fig. 11a–d). However, the effect of PBLD on cell cycle and apoptosis was not observed in *Pbld*-deficient MEFs (Supplementary Figs. 10e, f, 11e, f). This indicated that PBLD affected cell cycle and apoptosis may occur in cancer cells. More importantly, we conducted additional research on type I IFN response and viral replication interfered with the antibody-mediated IFNAR blocking in HeLa cells and MEFs as well as IFNAR blockade in mice to further support the specific antiviral effect of PBLD through type I IFN response, thereby highlighting the biological function of PBLD as a crucial regulator of IFN-I antiviral defense during viral infections, which serves potentially as a promising target for antiviral therapy.

NF-κB is a critical transcription factor needed for the production of IFNs and the inflammatory response to pathogen infection. A growing number of viruses has been reported to activate the NF-κB pathway[31–36]. In agreement with these findings, our study showed that PBLD activates NF-κB during viral infection. However, this is in contrast to published findings that PBLD greatly attenuates NF-κB transcriptional activity in intestinal epithelial cells (IECs) in dextran sulfate sodium (DSS)-induced colitis[21]. This implies that PBLD exert differences functions in the NF-κB signaling pathway through alternative mechanisms.

An increasing number of studies indicate that targeting the IKK complex is the key to regulate the response of the NF-κB signaling pathway by viral protein, such as the V protein of human parainfluenza virus type 2 (HPIV2) and F317L protein of African swine fever virus (ASFV)[37,38]. In addition, several host factors including fas-associated factor 1 (FAF1) and transferrin receptor 1 (TfR1) have been reported to participate in the inhibition of IKK activation and the subversion of NF-κB activation[39,40]. In this study, we have investigated the specific mechanism by which PBLD activates NF-κB after viral infection via blocking TRIM21. E3 ligase TRIM21 is a negative regulator of NF-κB signaling pathway via degradation of phosphorylated IKKβ[29,30]. We found that PBLD interacts with TRIM21 after viral infection, thereby blocking the degradation effect of TRIM21 on phosphorylated IKKβ, promoting the IKKs complex activation, subsequently enhancing the phosphorylation and degradation of IκBα, and ultimately activating the NF-κB/IFN-I signaling pathway and suppressing viral replication. Given that intervention in viral infectivity and modulation of host cell defense systems through targeting host factors necessary for virus replication are two main strategies for developing broad-spectrum antiviral drugs, based on our finding, PBLD/NF-κB pathway may be a target and strategy for antiviral direction.

One significant finding from our study is the inhibitory effect of Cedrelone on multiple virus replication. It is well known that small molecule chemical drugs are still the most powerful “weapon” against

https://doi.org/10.1038/s41467-024-54882-y

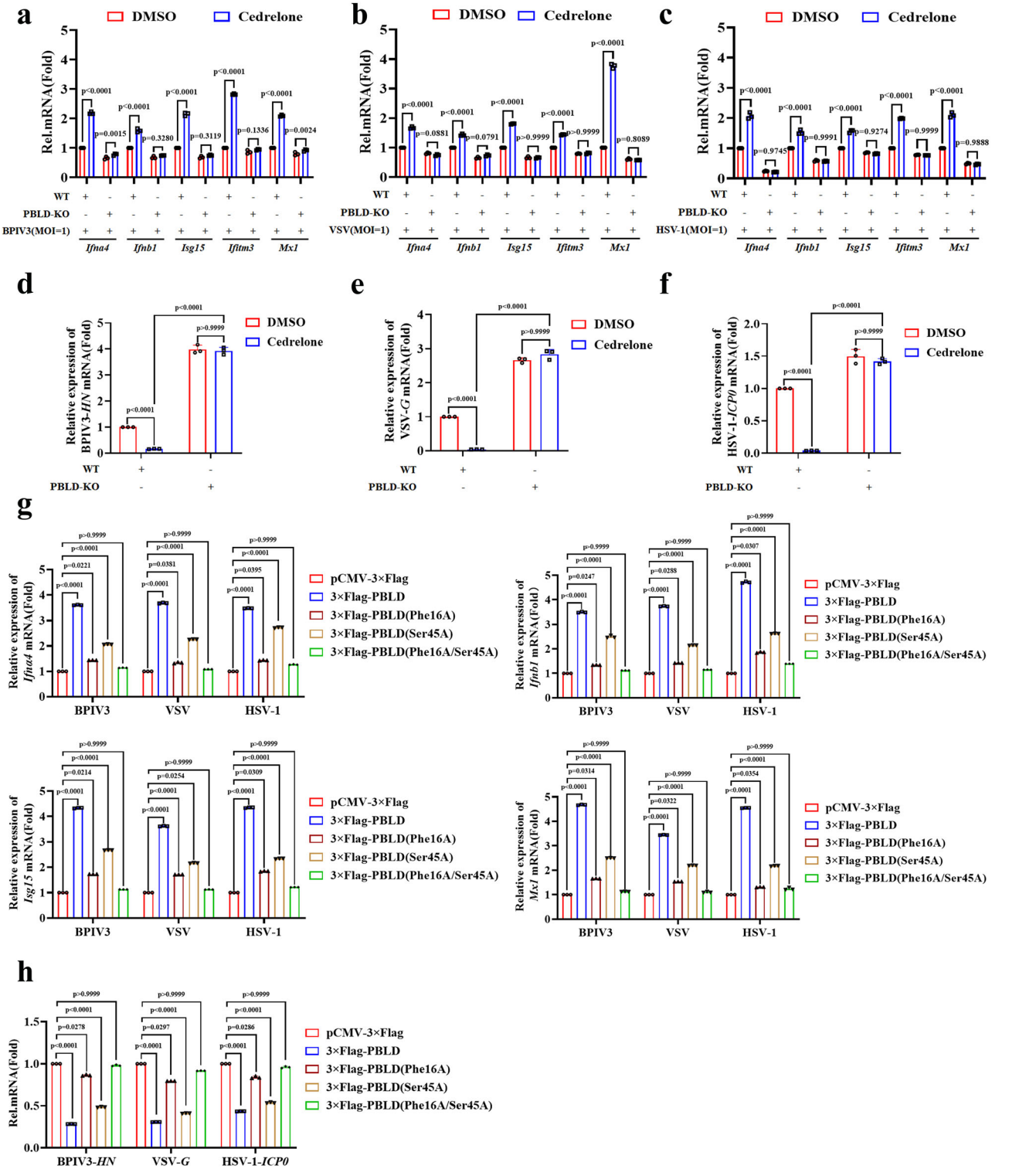

Fig. 7 | Cedrelone enhances the antiviral IFN-I immune response via the binding site at Ser 45 and Phe 16 of PBLD. Real-time PCR analysis the mRNA expression of IFNs and ISGs in BPIV3-infected MDBK cells (**a**), VSV (**b**) and HSV-1 (**c**)-infected HeLa cells as well as PBLD-KO MDBK and HeLa cell lines, then challenged with DMSO (vehicle control) and Cedrelone (1 μM) for 12 h, respectively. Real-time PCR analysis the mRNA levels of viral genes in BPIV3 (**d**), VSV (**e**), and HSV-1 (**f**) infected MDBK and HeLa cells or corresponding PBLD-KO cells, then challenged with DMSO (vehicle control) and Cedrelone (1 μM) for 12 h, respectively. **g** Real-time PCR analysis of the expression of IFNs and ISGs gene in PBLD-KO HeLa cell lines after introduced wild type PBLD and its mutates upon BPIV3, VSV or HSV-1 infection, then challenged with DMSO (vehicle control) and Cedrelone (1 μM) for 12 h, respectively. **h** Real-time PCR analysis of the expression of BPIV3-*HN*, VSV-*G* and HSV-1-*ICP0* gene in PBLD- KO HeLa cell lines after introduced wild type PBLD and its mutates upon BPIV3, VSV or HSV-1 infection, then challenged with DMSO (vehicle control) and Cedrelone (1 μM) for 12 h, respectively. All data are presented as mean ± SD, $n = 3$ biological independent experiments; two-way ANOVA for (**a**–**c**), one-way ANOVA (**d**–**h**). Source data are provided as a Source data file.

https://doi.org/10.1038/s41467-024-54882-y

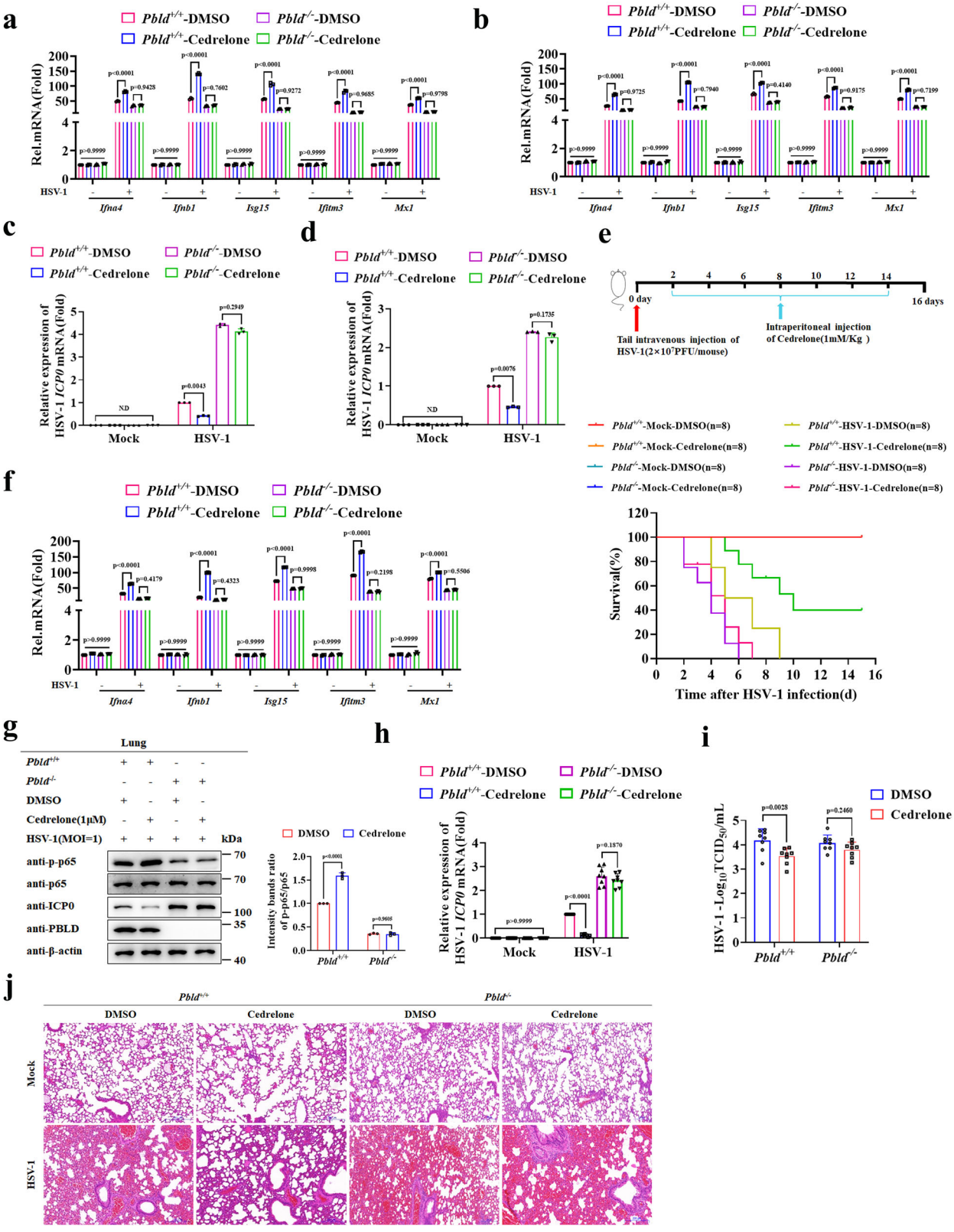

viral infections[41,42]. Broad-spectrum antiviral drugs can act on multiple viruses, and they have obvious advantages compared to specific antiviral drugs[43–45]. Cedrelone belongs to the class of compounds known as limonoids. Limonoids are a class of triterpenoids extracted from Neem, Citrus, Withania sominifera, and other plants are well-established antivirals and are known to inhibit the replication of human immunodeficiency virus (HIV), dengue virus, and Hepatitis C virus (HCV)[46–48]. However, the function of Cedrelone on virus replication remains unclear. In this study, we discover that Cedrelone has antiviral activity both in passaged cells and primary macrophages, as well as in vivo mouse models in a PBLD dependent way. Mechanistically, Cedrelone upregulates the PBLD expression, activates the NF-κB pathway and enhances the IFN-I immune response through the site at Ser 45 and Phe 16 of PBLD against multiple virus replication. These

Fig. 8 | Cedrelone promotes antiviral immunity in primary macrophages and attenuates HSV-1 infection in C57BL/6 J mice depending on PBLD. Real-time PCR analysis the mRNA levels of IFNs, ISGs and HSV-1 *ICP0* in PMs (**a**, **c**) and BMDMs (**b**, **d**) from *Pbld*$^{+/+}$ and *Pbld*$^{-/-}$ mice infected with HSV-1 (MOI = 1) or mock infection, respectively, and administered with DMSO (vehicle control) or Cedrelone (1 μM) for 12 h. **e** Schematic of the workflow of experiments: *Pbld*$^{+/+}$ and *Pbld*$^{-/-}$ mice were tail intravenous injected with HSV-1(2×10^7 PFU/mouse) or mock inoculated. After 2 days of infection, each group of mice was treated with intraperitoneal injections of Cedrelone at a concentration of 1 mM/Kg of body weight at 2 days interval, and DMSO serves as vehicle control. The survival curves of age- and sex-matched littermates was estimated by the Kaplan–Meier method and compared by two-side log-rank test ($n = 8$ for each group). P = 0.3534 for *Pbld*$^{-/-}$ plus DMSO versus *Pbld*$^{-/-}$ plus Cedrelone. Real-time PCR analysis the mRNA levels of IFNs, ISGs (**f**) and HSV-1 *ICP0* (**h**), and western blotting analysis of the indicated protein expression (**g**) in lung of HSV-1 (2×10^7 PFU/mouse) infected *Pbld*$^{+/+}$ and *Pbld*$^{-/-}$ mice, then challenged with DMSO and Cedrelone (1 mM/Kg) for 2 days, respectively. **i** Virus titer detection of HSV-1 determined by $TCID_{50}$ in lung of HSV-1 infected *Pbld*$^{+/+}$ and *Pbld*$^{-/-}$ mice, then challenged with DMSO and Cedrelone for 2 days, respectively. **j** Hematoxylin and eosin stained images of lung from *Pbld*$^{+/+}$ and *Pbld*$^{-/-}$ mice with HSV-1 infection, and then administered with DMSO or Cedrelone for 2 days, respectively. Scale bars, 100 μm. N.D not detected. Data in (**a**–**d**, **f**, **h**, **i**) are presented as mean ± SD, $n = 3$ for (**a**–**d**, **f**), $n = 8$ for (**h**, **i**) biological independent experiments; two-way ANOVA. Data in (**g**, **j**) are representative from three independent experiments. The gray intensity of the bands in data (**g**) presented as mean ± SD from three independent experiments were analyzed using ImageJ software. Statistical analysis of intensity quantitation in data (**g**) was performed by two-way ANOVA. Source data are provided as a Source data file.

data revealed that the Cedrelone, targeting PBLD, has the potential to be further developed as a resource of broad-spectrum antiviral drugs.

It has been reported that Cedrelone induces cell cycle arrest and apoptosis in cancer cells[25,49]. As such, we assessed that Cedrelone at a concentration of 1 μM could slightly trigger G2/M cell cycle arrest (Supplementary Fig. 12a, b) and promote virus induced apoptosis in HeLa cells after treatment for 24 h by flow cytometry (Supplementary Fig. 13a, b). However, this phenomenon was not significantly observed in Cedrelone treated MEFs (Supplementary Figs. 12c, d, 13c, d). Collectively, although the use of HeLa cells to study the antiviral effects of Cedrelone is not a good model, the antiviral effects of Cedrelone have also been confirmed in MEFs, primary macrophages, and mouse models, which further support the specific antiviral effect of Cedrelone. Furthermore, toxicity is one of the limiting factors in the therapeutic application of many drugs despite their known antiviral activities. For comparison, SI of Cedrelone was found to be ~2, demonstrating a much lower safety profile of this drug. Although the SI value of Cedrelone is low, it is possible to potentially minimize the toxicity of drugs by decreased acetylation of Cedrelone, or removing the toxic compound(s) using certain chemical method(s), chemical modification (N6 -benzyladenosine) and use of nanogels drug delivery systems to increase SI[50–53]. More importantly, this study confirmed that PBLD is an ideal target molecule for antiviral drug research. It is expected to predict small molecule compounds that activate or promote its stability based on its crystal structure, providing ideas and clues for in-depth exploration of antiviral drug research based on PBLD.

In summary, our study unveils the biological function of PBLD in activating the NF-κB signaling pathway, thereby enhancing the IFN-I-mediated antiviral defense. Furthermore, we discover that Cedrelone enhances the IFN-I response against multiple virus replication depending on PBLD (Fig. 9). Therefore, our findings simulate a potential combination model of PBLD as a therapeutic target for Cedrelone antiviral drug therapy, which may provide a strategy for the development of targeted broad-spectrum antiviral drugs.

Methods

Ethics statement

This study complied with all of the relevant ethical regulations. All mice experiments were approved by the Institutional Animal Care and Use Committees at Shandong Normal University (permission number: AEECSDNU2023023).

Cells and viruses

HeLa cells (CCL-2, ATCC), Madin-Darby bovine kidney (MDBK) cells (CCL-22, ATCC) were obtained from the Cell Bank of Type Culture Collection of the Chinese Academy of Sciences (Shanghai, China) and stored in our laboratory. All cells were maintained in Dulbecco's Modified Eagle's Medium (DMEM; VivaCell, C3110-0500) supplemented with 10% fetal bovine serum (FBS) (TransGen Biotech, FS301-02, China) and antibiotics (100 U/mL penicillin and 100 mg/mL streptomycin sulfate) (New Cell & Molecular Biotech Co., Ltd) at 37 °C with 5% CO_2. The BEFV (Shandong/China/2011)[54], BPIV3 (No. CGMCC9992) strain[55], were isolated and stored at Shandong Normal University, Jinan, Shandong Province, China. Sendai virus (SeV), Vesicular stomatitis virus (VSV) (ATCC VR-1238) and Herpes simplex virus type 1 (HSV-1) (Kos strain) were kindly gifted from Pro. Y. Gao (Changchun Veterinary Research Institute).

Antibodies, inhibitors and reagents

Antibodies against β-actin(AB0035)(1:5000), ISG15(CY9357) (1:1000), IFITM3(CY7091) (1:1000), IKK alpha (CY5735) (1:1000), IKK beta (CY5636) (1:1000), IKB alpha (CY5026) (1:1000), phospho-IKB alpha (S32) (CY5572) (1:1000), p50(CY5040) (1:1000), TRIM21(AB3412) (1:1000), IFNARI (CY5463)(1:1000 for Western blot; 10 μg/mL for cell blocking), IgG (Human)(CY6900)(1:1000 for Western blot; 10 μg/mL for cell blocking), STAT1(CY5227)(1:2000), phospho-STAT1(CY5702) (1:2000), VSV-G(AB0053) (1:5000) were purchased from Abways Biotechnology Co., Ltd. Phospho-IKKαβ (S176/S177) (AF3014(1:1000)) were purchased from Affinity. Rabbit anti-GFP (AE011)(1:1000) were purchased from Abclonal. Rabbit anti-DYKDDDDK Tag (D6W5B) (#14793) (1:1000), rabbit anti-HA Tag (C29F4) (#3724) (1:1000), NF-κB p65(#8242) (1:1000), phospho-NF-κB p65 (Ser536) (#3033) (1:1000) antibody were purchased from Cell Signaling Technology. Anti-PBLD (sc-101502) (1:1000) (human/mouse cells), anti-HSV-1 ICP0 (sc-53070) (1:1000), HSV-1 UL42 (sc-53331) (1:1000), HSV-1 gB (sc-56987) (1:1000) were purchased from Santa Cruz Biotechnology and anti-PBLD (68317-1-Ig) (1:1000) (bovine cells), mouse IgG (B900620, 500/250 μg/mouse) were purchased from proteintech. Mouse IFNAR1(HY-P99137, 500/250 μg/mouse) was purchased from Med Chem Express. Mouse anti-BEFV N (1:1000), mouse anti-BPIV3 HN (1:1000), mouse anti-SeV NP (1:1000) were prepared and stored at Shandong Normal University, Jinan, Shandong Province, China. Goat anti-rabbit IgG (H + L) (115-005-003) (1:5000) and goat anti-mouse IgG (H + L) (111-005-003) (1:5000) horseradish peroxidase (HRP)-conjugated secondary antibodies were purchased from Jackson ImmunoResearch Laboratories Inc., USA. Cross-adsorbed secondary antibody, Alexa Fluor™ 594 (A-11005) (1:500), Protein A/G magnetic beads (88803) was obtained from ThermoFisher. Dimethyl sulfoxide (DMSO, 472301) and chloroquine diphosphate salt (CQ, C6628) were purchased from Sigma-Aldrich. Anti-DDDDK-tag magnetic beads (M185-11), anti-HA-tag magnetic beads(M180-11) were purchased from MBL. Gastrodin (HY-N0115), MG132(HY-13259C), MG101 (HY-18964) and QNZ (HY-13812) were purchased from Med Chem Express. Attractene transfection reagent (301007) was obtained from QIAGEN, USA. Poly[I:C] (tlrl-picwlv), Poly[dA:dT](tlrl-patn) were purchased from Invivogen. Cedrelone (1254-85-9) was purchased from TargetMOI.

Mice

The *Pbld1* and *Pbld2* genes in mice encode PBLD proteins[56]. To generate murine heterozygotes with a C57BL/6 background, the CRISPR/

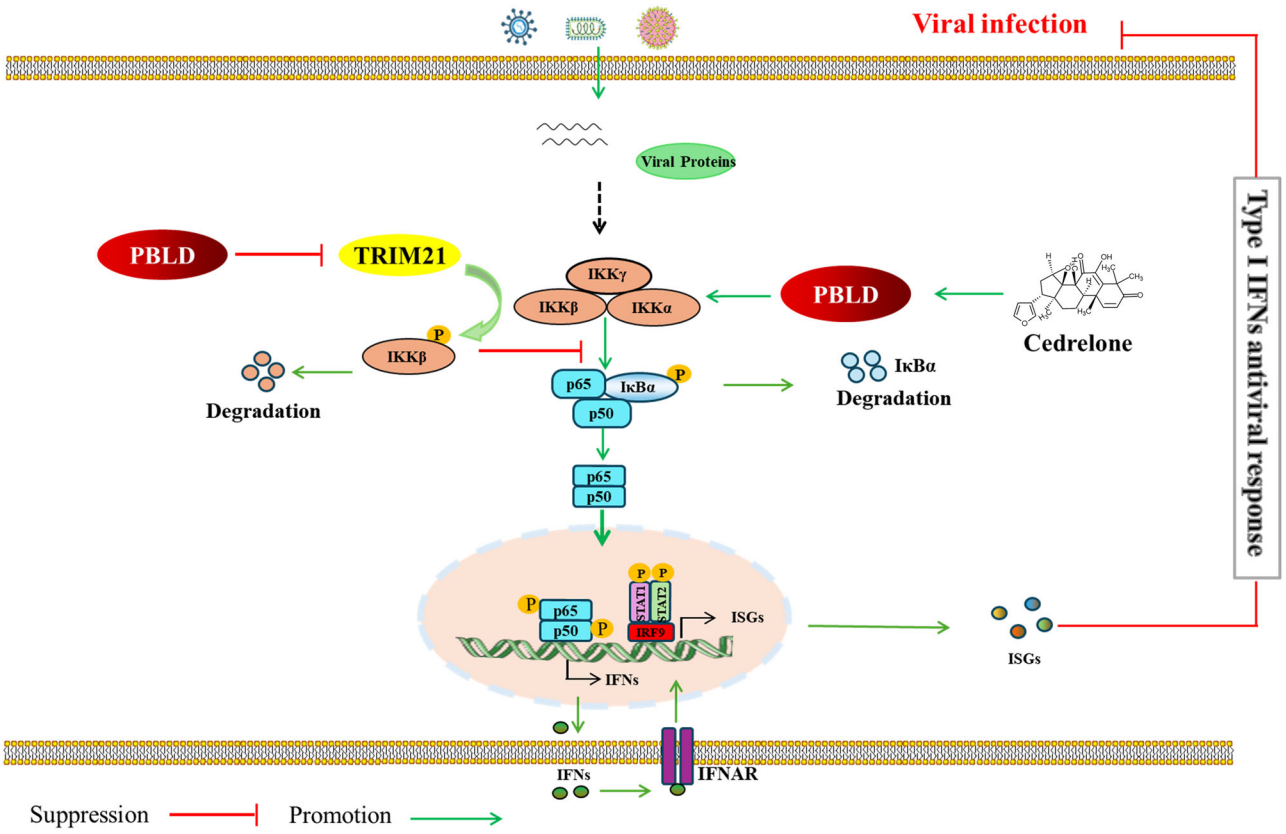

Fig. 9 | Model depicting PBLD and Cedrelone inhibit viral replication via activating the NF-κB-mediated IFN-I signaling response. Upon viral infection, PBLD interacts with TRIM21, thereby blocking the degradation effect of TRIM21 on phosphorylated IKKβ, promoting IKKs complex activation, and ultimately activating the NF-κB signaling pathway and enhancing the IFN-I-mediated antiviral defense. Furthermore, Cedrelone effectively promotes antiviral IFN-I immune response by increasing the PBLD protein expression and activating the NF-κB pathway.

Cas9 gene editing system was utilized with the help of Guangzhou Cyagen Biosciences Inc. The *Pbld*$^{-/-}$ mice exhibited normal growth and development, similar to their wild-type littermates. Both sexes and eight-weeks old mice were used in the experiments. Same sex littermates were randomly assigned to the experimental groups. The mice were bred under specific pathogen-free conditions at the Shandong Normal University for Animal Research Center, housed at an ambient temperature of ~24 °C, a humidity of 40–60%, and a light/dark cycle of 12 h.

Isolation of mouse PMs, BMDMs and MEFs

Mouse peritoneal macrophages (PMs) were acquired from the peritoneal lavage 3 days after intraperitoneal injection of starch solution (Sigma Aldrich, 232-679-6). The fluid containing PMs was aspirated from the peritoneum after agitation and were cultured in DMEM supplemented with 10% fetal calf serum (FBS), and non-adherent cells were washed away with PBS before further use.

Bone marrow-derived macrophages (BMDMs) were isolated from the tibia and femur by rinsing with PBS and filtering through a 40-μm cell strainer. Subsequently, the red blood cell lysate was used to eliminate red blood cells. The cells were then collected and resuspended in RPMI-1640 medium supplemented with 10% FBS for 16 h. After that, adherent cells were discarded. The BMDMs cells were incubated for 7 days at 37 °C and 5% CO_2 in medium containing 20 ng/mL macrophage colony-stimulating factor (GM-CSF) (Novoprotein, CJ46, Suzhou, China).

Mouse embryonic fibroblasts (MEFs) were generated from pregnant females for 13-day-old of WT and *Pbld*$^{-/-}$ mice. The fetuses were dissected out the fetal viscera, head, and limbs were excised from embryos, and the rest of the other embryonic tissues were minced and incubated with 0.25% trypsin for 30 min at 37 °C. The MEFs were cultured in DMEM supplemented with 10% FCS, 100 U/mL penicillin, and 100 μg/mL streptomycin at 37 °C under 5% CO_2.

Plasmids construction and small interfering RNAs

Homo sapiens PBLD coding sequence (GenBank accession no. NM_001033083.2) or bovine PBLD coding sequence (GenBank accession no. XM_024986592.1) was amplified by PCR and cloned into the pCMV-Flag-N vector and pLVX-IRES-Puro vector, respectively. The primer pairs used for PBLD and its mutants amplification at Ser 45 and Phe 16 of PBLD, TRIM21, TRIM21-△RING are listed in Supplementary Table 1. Additionally, the small interfering RNA (siRNA) sequences of siPBLD, siNF-κB or siTRIM21 used in the study are shown in Supplementary Table 1. All siRNAs were synthesized by GenePharma Biological Technology Co., Ltd.

Generation of stably expressed PBLD or PBLD knockout (KO) cell lines through CRISPR–Cas9 system

The MDBK or HeLa cell lines stably expressed PBLD were obtained with the pLVX-IRES-puro lentiviral vector system, and PBLD knockout MDBK or HeLa cell lines were generated using the lenti-CRISPR/Cas9-V2 system[57]. The guide RNA (gRNA) sequences for PBLD, listed in Supplementary Table 1, were designed via the online browser CRISPR Direct (http://crispr.dbcls.jp/). Single clonal knockout cells treated with puromycin (Solarbio, P8230) were isolated and subsequently confirmed by immunoblot analysis.

Real-time quantitative RT-PCR

Total RNA was extracted from cells or tissue samples according to the instructions of RNA extraction kit (Foregene, RE-03111), and

then cDNA was produced using reverse transcription kit (Accurate, AG11706). The expression of IFNs, ISGs and viral genes were determined by quantitative reverse transcription-PCR (RT-qPCR) using the SYBR Green Master Mix (Vazyme, Q111-02) with the primer pairs provided in Supplementary Table 2. As the transcript of GAPDH is virtually degraded by the HSV-1 protein, it is not a sufficient housekeeping gene to use for HSV-1 infection[58]. The relative expression of the target genes was normalized to either β-actin for HSV-1 infection or GAPDH for BPIV3 infected MDBK cells, respectively. The relative mean mRNA fold changes relative to the control were calculated using the $2^{-\Delta\Delta Ct}$ method.

Immunoprecipitation and Western blot analysis

The indicated plasmids were transfected into HeLa cells with Attractene Transfection Reagent (QIAGEN, 301007) as per the manufacturer's protocol. The cells were then collected and lysed for 15 min with ice-cold low-salt lysis buffer (Thermo Fisher Scientific, 78441) supplemented with inhibitors for protease and phosphatases (New Cell & Molecular Biotech Co.,Ltd, P002). The supernatant of whole-cell extracts was incubated with indicated Magarose Beads (Smart-Lifesciences, SM009001) overnight on a rotor at 4 °C. The beads were washed 5 times with low-salt lysis buffer. Subsequently, the immunoprecipitates were resuspended in 1× SDS loading buffer (Elabscience, E-BC-R288) and boiled for 5 min. The released proteins were analyzed by SDS-PAGE electrophoresis (Epizyme, PG113) and transferred onto polyvinylidene difluoride (PVDF) membranes (LABSELECT, TM-PVDF-R-45). The membranes were then blocked and incubated with the indicated antibodies. The proteins were detected using enhanced chemiluminescence (ECL) detection (Shandong Sparkjade Biotechnology, ED0015-C) with an imaging system (Tanon Science & Technology Co., Ltd, Shanghai, China).

Identification of PBLD binding proteins by mass spectrometry

PBLD-overexpression of HeLa cell lines (Flag-PBLD) and control cell lines (Vector) infected with BPIV3 (MOI = 1) for 12 h. Cell lysate was immunoprecipitated with anti-Flag antibody–conjugated agarose beads overnight. Immunoprecipitated protein were subjected to 12.5% SDS-PAGE gel (epizyme, PG113) with one biological replicates. After Coomassie Brilliant Blue staining, we excised the band of PBLD binding group and control group. Subsequently, the purified proteins were digested by trypsin and analyzed by Jingjie PTM BioLabs (Hangzhou, China). For in-gel tryptic digestion, gel pieces were destained in 50 mM NH_4HCO_3 in 50% acetonitrile (v/v) until clear. After dehydrated with 100% acetonitrile for three times, gel pieces were rehydrated with 10 ng/μL trypsin resuspended in 50 mM NH_4HCO_3 on ice for 1 h. Excess liquid was removed and gel pieces were digested with trypsin at 37 °C overnight. Peptides extracted with 50% acetonitrile/5% formic acid, followed by 100% acetonitrile were subjected to NSI source followed by tandem mass spectrometry (MS/MS) in Q Exactive™ Plus (Thermo) coupled online to the UPLC. The electrospray voltage applied was 2.2 kV. The m/z scan range was 350–1800 for full scan, and intact peptides were detected in the Orbitrap at a resolution of 70,000. Peptides were then selected for MS/MS using NCE setting as 28 and the fragments were detected in the Orbitrap at a resolution of 17,500. A data-dependent procedure that alternated between one MS scan followed by 20 MS/MS scans with 15.0 s dynamic exclusion. Automatic gain control (AGC) was set at 5E4. The resulting MS/MS data were processed using Proteome Discoverer 2.1. Tandem mass spectra were searched against human database. Trypsin/P was specified as cleavage enzyme allowing up to 2 missing cleavages. Mass error was set to 10 ppm for precursor ions and 0.02 Da for fragment ions. Carbamidomethyl on Cys were specified as fixed modification and oxidation on Metwas specified as variable modification. Peptide confidence was set at high, and peptide ion score was set >20.

Flow cytometry for cell-cycle and apoptosis analysis

Cell cycle analysis kit (Beyotime, C1052) was used in cell cycle assay. Cells were trypsinized, washed in PBS, fixed in 70% ethanol, and stained with propidium iodide/RNase staining buffer. Individual cells in different phases of the cell cycle were characterized for forward and side scatter and DNA content (propidium iodide intensity) was determined in 10,000 cells as measured by flow cytometry (excitation at 488 nm, emission measured using 600-nm bandpass filter) with a Becton Dickinson Fortessa flow cytometer, and populations of G1, S, and G2/M phase cells were determined with the FlowJo software.

Cell apoptosis was analyzed by flow cytometry with a Annexin V-FITC/PI apoptosis detection kit (Yeasen, 40302ES50). Cells were collected with trypsin without EDTA and then stained with Annexin V-FITC and PI in accordance with the manufacturer's instructions. Then cells were analyzed by flow cytometry. The relative proportion of early apoptotic cells and apoptotic cells was combined as the target of our comparison. Flow cytometry analysis was performed using FlowJo software.

Cell viability assay

HeLa cells were seeded in 96-well plates and treated with various concentrations of MG101, QNZ, or Cedrelone, respectively. Cell viability was assessed using the enhanced cell counting kit-8 (CCK-8, Yeasen, 40203ES) following the manufacturer's instructions. Specifically, after a 24-h incubation, CCK-8 solution mixed with 100 μL of DMEM was added to each well and incubated at 37 °C for 1 h. The absorbance at 450 nm was then measured using a microplate reader.

Drug treatment

The cells were planted evenly into a 6-well plate at a density of 2.5×10^6 cells per well, and MG101 (20 μM), QNZ (10 μM), Cedrelone (0.5, 1 μM) or Gastrodin (50 μM) was added to the cells. After 4 h of drug treatment, remove the culture medium and infect the cells with the indicated viruses. After that, replace the medium with corresponding concentration of drug. Then, collect the cells at indicated time for subsequent experiments.

Blocking of IFNAR receptor in vitro

Cells were treated with 10 μg/mL anti-IFNAR antibody or IgG isotype control at a concentration of 10 μg/mL for 2 h at 37 °C. After 2 h, the antibodies were removed, and cells were infected with indicated virus for 1 h. Following removal of the viral infection inoculum, the medium containing 10 μg/mL antibody was returned to the cells.

IFNAR blockade in vivo

Pbld$^{+/+}$ and *Pbld*$^{-/-}$ mice were treated with 500 μg/mouse intraperitoneally with neutralizing antibody (nAb) to IFNAR or mouse IgG isotype control at the following time points (and doses): day −1 (500 μg/mouse), day 0 (500 μg/mouse), day 2 (250 μg/mouse) and day 4 (250 μg/mouse)[59]. Uninfected control mice were similarly treated in parallel. On day 0, mice were challenged with HSV-1 (2×10^7 pfu per mouse). Disease progression and mortality were monitored daily.

Enzyme-linked immunosorbent assay (ELISA)

The concentrations of mouse IFN-α (Solarbio, SEKM-0359,) and IFN-β (Multisciences (Lianke), EK2236) in serum were measured by ELISA kits, according to the manufacturer's instructions.

Virus challenge and $TCID_{50}$ assay for virus titers

The HeLa, MDBK cell lines with PBLD overexpression or knockout, and *Pbld*-deficient MEFs, PMs and BMDMs as well as control cell lines, were infected with BPIV3, VSV or HSV-1 at MOI of 1 for the indicated time. Subsequently, samples were collected and stored at −80 °C. To determine viral titers, the samples underwent three

cycles of freeze-thawing and 10-fold dilutions of the virus inoculum were prepared, subsequently subjected to the 50% Tissue Culture Infective Dose ($TCID_{50}$) assay in 96-well plates. The viral titter, measured in $lgTCID_{50}$/mL, was determined via the Reed-Muench method.

Molecular docking

The structure of Cedrelone was obtained from the PubChem database (https://pubchem.ncbi.nlm.nih.gov/). The structural model of PBLD was generated using the modeling servers SWISS-MODEL (https://swissmodel.expasy.org/). Molecular docking studies were performed in Autodock vina[60] (https://vina.scripps.edu/) to find out the interactions of Cedrelone with the PBLD proteins. The water molecules were removed and hydrogen addition during protein preparation, followed by adding the Gasteiger charge and grid-box-based docking was performed as per the instructions. Moreover, the center of combined area was x = −2.178, y = −1.106, z = −1.598, spacing 1.000 (size x = 126.0; y = 100.0; z = 86.0). Molecular graphic figures were made using the molecular visualization system PyMOL Molecular Graphics System (2.3, Schrödinger, German) (www.pymol.org). The chemical structure of Cedrelone was rendered using ChemDraw (http://chemdraw.djajy.cn/), adhering to the standards of Nature Chemistry (http://www.nature.com/authors/guides/NR_chemdraw_stylesheet.cds).

Antiviral activity test

To determine the antiviral activity of Cedrelone, cells were seeded in a 96-well plate and infected with indicated viruses in DMEM growth medium. Next, virus-infected cells were treated with serially diluted Cedrelone. After 24 h, cell viability was determined via the CCK-8 kit (Yeasen, 40203ES). The CC_{50} value of Cedrelone was defined as the concentration inducing 50% cell death. The IC_{50} of samples was defined as the concentration leading to 50% effective inhibition. Selective index (SI) was determined by the ratio of the CC_{50} to IC_{50}.

Animal studies

Eight-week-old C57BL/6 (B6) mice, both $Pbld^{+/+}$ and $Pbld^{-/-}$ and sex matched littermates were used in the experiments. Whole blood and tissues were collected from these mice before and after HSV-1 infection. Viral replication and infectivity were assessed by detection of viral RNA copies and viral titers; the degree of innate immunity response in mice was evaluated by ELISA and RT-qPCR; the pathogenicity of HSV-1 in mice was measured through histopathology.

Statistical analyses

Statistical analyses were performed using Graphpad Prism software 8.0 (GraphPad Software, La Jolla, CA, United States). The data were presented as mean values ± standard deviation (SD) from at least three independent experiments. Student's t-test was employed to compare values between the two groups. For multiple comparisons, two-way analysis of variance (ANOVA), and one-way ANOVA was performed. P value below 0.05 was considered statistically significant.

Reporting summary

Further information on research design is available in the Nature Portfolio Reporting Summary linked to this article.

Data availability

Raw mass spectrometry data have been deposited to the ProteomeXchange Consortium via PRIDE partner repository under accession code PXD056953. All data supporting the findings of this study are available within the article, and the data generated in this study including uncropped and unprocessed scans of the representative blots shown in the Figures are provided in the Supplementary Information and Source data file. Source data are provided with this paper.

References

1. Morens, D. M. & Fauci, A. S. Emerging pandemic diseases: how we got to COVID-19. *Cell* **182**, 1077–1092 (2020).
2. Baker, R. E. et al. Infectious disease in an era of global change. *Nat. Rev. Microbiol.* **20**, 193–205 (2022).
3. Mesev, E. V., LeDesma, R. A. & Ploss, A. Decoding type I and III interferon signalling during viral infection. *Nat. Microbiol.* **4**, 914–924 (2019).
4. Wu, J. & Chen, Z. J. Innate immune sensing and signaling of cytosolic nucleic acids. *Annu. Rev. Immunol.* **32**, 461–488 (2014).
5. Ablasser, A. & Hur, S. Regulation of cGAS- and RLR-mediated immunity to nucleic acids. *Nat. Immunol.* **21**, 17–29 (2020).
6. Yu, H., Lin, L., Zhang, Z., Zhang, H. & Hu, H. Targeting NF-κB pathway for the therapy of diseases: mechanism and clinical study. *Signal Transduct. Target Ther.* **5**, 209 (2020).
7. Oeckinghaus, A. & Ghosh, S. The NF-kappaB family of transcription factors and its regulation. *Cold Spring Harb. Perspect. Biol.* **1**, a000034 (2009).
8. Sun, S. C. The noncanonical NF-κB pathway. *Immunol. Rev.* **246**, 125–140 (2012).
9. Hayden, M. S., West, A. P. & Ghosh, S. SnapShot: NF-kappaB signaling pathways. *Cell* **127**, 1286–1287 (2006).
10. Kolesnichenko, M. et al. Transcriptional repression of NFKBIA triggers constitutive IKK- and proteasome-independent p65/RelA activation in senescence. *Embo J.* **40**, e104296 (2021).
11. Israël, A. The IKK complex, a central regulator of NF-kappaB activation. *Cold Spring Harb. Perspect. Biol.* **2**, a000158 (2010).
12. Hinz, M. & Scheidereit, C. The IκB kinase complex in NF-κB regulation and beyond. *EMBO Rep.* **15**, 46–61 (2014).
13. Valentine, R. et al. Epstein-Barr virus-encoded EBNA1 inhibits the canonical NF-kappaB pathway in carcinoma cells by inhibiting IKK phosphorylation. *Mol. Cancer* **9**, 1 (2010).
14. McNamara, A. J., Brooks, A. D. & Danthi, P. The reovirus σ3 protein inhibits NF-κB-dependent antiviral signaling. *J. Virol.* **96**, e0051522 (2022).
15. Pham, A. M. & TenOever, B. R. The IKK kinases: operators of antiviral signaling. *Viruses* **2**, 55–72 (2010).
16. Wu, F., Niu, Z., Zhou, B., Li, P. & Qian, F. PSMB1 Negatively regulates the innate antiviral immunity by facilitating degradation of IKK-ε. *Viruses* **11**, 99 (2019).
17. Yang, H. et al. The host antiviral protein SAMHD1 suppresses NF-κB activation by interacting with the IKK complex during inflammatory responses and viral infection. *J. Biol. Chem.* **299**, 104750 (2023).
18. Iriyama, C., Matsuda, S., Katsumata, R. & Hamaguchi, M. Cloning and sequencing of a novel human gene which encodes a putative hydroxylase. *J. Hum. Genet.* **46**, 289–292 (2001).
19. Herde, P. & Blankenfeldt, W. The purification, crystallization and preliminary structural characterization of human MAWDBP, a member of the phenazine biosynthesis-like protein family. *Acta Crystallogr. Struct. Biol. Cryst. Commun.* **62**, 546–549 (2006).
20. Zhao, X. et al. Evaluation of p38 MAPK pathway as a molecular signature in ulcerative colitis. *J. Proteome Res.* **10**, 2216–2225 (2011).
21. Chen, S. et al. Epithelial PBLD attenuates intestinal inflammatory response and improves intestinal barrier function by inhibiting NF-κB signaling. *Cell Death Dis.* **12**, 563 (2021).
22. Han, L. et al. PBLD inhibits angiogenesis via impeding VEGF/VEGFR2-mediated microenvironmental cross-talk between HCC cells and endothelial cells. *Oncogene* **41**, 1851–1865 (2022).
23. Li, D. M. et al. MAWBP and MAWD inhibit proliferation and invasion in gastric cancer. *World J. Gastroenterol.* **19**, 2781–2792 (2013).
24. Gopalakrishnan, G., Pradeep Singh, N. D., Kasinath, V., Malathi, R. & Rajan, S. S. Photooxidation of cedrelone, a tetranortriterpenoid from Toona ciliata. *Photochem. Photobiol.* **72**, 464–466 (2000).

25. Cazal, C. M. et al. Evaluation of effect of triterpenes and limonoids on cell growth, cell cycle and apoptosis in human tumor cell line. *Anticancer Agents Med. Chem.* **10**, 769–776 (2010).
26. Fuzer, A. M. et al. Effects of limonoid cedrelone on MDA-MB-231 breast tumor cells in vitro. *Anticancer Agents Med. Chem.* **13**, 1645–1653 (2013).
27. Wu, J., Niu, Q., Yuan, J., Xu, X. & Cao, L. Novel compound cedrelone inhibits hepatocellular carcinoma progression via PBLD and Ras/Rap1. *Exp. Ther. Med.* **18**, 4209–4220 (2019).
28. Lindqvist, R. et al. Fast type I interferon response protects astrocytes from flavivirus infection and virus-induced cytopathic effects. *J. Neuroinflamm.* **13**, 277 (2016).
29. Wada, K., Niida, M., Tanaka, M. & Kamitani, T. Ro52-mediated monoubiquitination of IKK{beta} down-regulates NF-{kappa}B signalling. *J. Biochem.* **146**, 821–832 (2009).
30. Niida, M., Tanaka, M. & Kamitani, T. Downregulation of active IKK beta by Ro52-mediated autophagy. *Mol. Immunol.* **47**, 2378–2387 (2010).
31. Chan, J. K. & Greene, W. C. Dynamic roles for NF-κB in HTLV-I and HIV-1 retroviral pathogenesis. *Immunol. Rev.* **246**, 286–310 (2012).
32. Willis, K. L., Langland, J. O. & Shisler, J. L. Viral double-stranded RNAs from vaccinia virus early or intermediate gene transcripts possess PKR activating function, resulting in NF-kappaB activation, when the K1 protein is absent or mutated. *J. Biol. Chem.* **286**, 7765–7778 (2011).
33. Hävemeier, A. et al. Activation of NF-κB by the Kaposi's sarcoma-associated herpesvirus K15 protein involves recruitment of the NF-κB-inducing kinase, IκB kinases, and phosphorylation of p65. *J. Virol.* **88**, 13161–13172 (2014).
34. Marino-Merlo, F. et al. HSV-1-induced activation of NF-κB protects U937 monocytic cells against both virus replication and apoptosis. *Cell Death Dis.* **7**, e2354 (2016).
35. Kong, F. et al. Hepatitis B virus core protein mediates the upregulation of C5α receptor 1 via NF-κB pathway to facilitate the growth and migration of hepatoma cells. *Cancer Res. Treat.* **53**, 506–527 (2021).
36. Santoro, M. G., Rossi, A. & Amici, C. NF-kappaB and virus infection: who controls whom. *Embo J.* **22**, 2552–2560 (2003).
37. Kitagawa, Y. et al. Human parainfluenza virus type 2 V protein inhibits TRAF6-mediated ubiquitination of IRF7 to prevent TLR7- and TLR9-dependent interferon induction. *J. Virol.* **87**, 7966–7976 (2013).
38. Yang, J. et al. African swine fever virus F317L protein inhibits NF-κB activation to evade host immune response and promote viral replication. *mSphere* **6**, e0065821 (2021).
39. Park, M. Y. et al. FAF1 suppresses IkappaB kinase (IKK) activation by disrupting the IKK complex assembly. *J. Biol. Chem.* **282**, 27572–27577 (2007).
40. Kenneth, N. S., Mudie, S., Naron, S. & Rocha, S. TfR1 interacts with the IKK complex and is involved in IKK-NF-κB signalling. *Biochem. J.* **449**, 275–284 (2013).
41. Janeba, Z. Development of small-molecule antivirals for Ebola. *Med. Res. Rev.* **35**, 1175–1194 (2015).
42. Yang, Y. et al. Discovery, optimization, and target identification of novel potent broad-spectrum antiviral inhibitors. *J. Med. Chem.* **62**, 4056–4073 (2019).
43. Adalja, A. & Inglesby, T. Broad-spectrum antiviral agents: a crucial pandemic tool. *Expert Rev. Anti Infect. Ther.* **17**, 467–470 (2019).
44. Zelikin, A. N. & Stellacci, F. Broad-spectrum antiviral agents based on multivalent inhibitors of viral infectivity. *Adv. Health. Mater.* **10**, e2001433 (2021).
45. Martinez, J. P., Sasse, F., Brönstrup, M., Diez, J. & Meyerhans, A. Antiviral drug discovery: broad-spectrum drugs from nature. *Nat. Prod. Rep.* **32**, 29–48 (2015).
46. Yu, J. H. et al. Limonoids with anti-HIV activity from cipadessa cinerascens. *J. Nat. Prod.* **78**, 1243–1252 (2015).
47. Cheng, Y. B. et al. Limonoids from the seeds of swietenia macrophylla with inhibitory activity against dengue virus 2. *J. Nat. Prod.* **77**, 2367–2374 (2014).
48. Kouam, A. F. et al. Inhibitory activity of limonoids from khaya grandifoliola C.DC (meliaceae) against hepatitis C virus infection in vitro. *Avicenna J. Phytomed.* **11**, 353–366 (2021).
49. Cao, Y., Zhang, L. & Wang, Y. Antitumor activity of Cedrelone in temozolomide-resistant human glioma cells is accompanied by mitochondrial mediated apoptosis, inhibition of angiogenesis, cell cycle disruption and modulation of ERK/MAPK signalling pathway. *J. BUON* **24**, 1204–1209 (2019).
50. Becceneri, A. B. et al. Acetylation of cedrelone increases its cytotoxic activity and reverts the malignant phenotype of breast cancer cells in 3D culture. *Chem. Biol. Interact.* **316**, 108920 (2020).
51. Made Ratih, G. A. et al. Phytochemicals of Gandarusa (Justicia gendarussa) and its preparations. *Nat. Prod. Commun.* **14**, 1934578X19851406 (2019).
52. Oslovsky, V. E. et al. Fluorination of naturally occurring N^6-benzyladenosine remarkably increased its antiviral activity and selectivity. *Molecules* **22**, 1219 (2017).
53. van Gent, M. E. et al. Encapsulation into hyaluronic acid-based nanogels improves the selectivity index of the snake cathelicidin Ab-Cath. *Nanomed. Nanotechnol. Biol. Med.* **52**, 102694 (2023).
54. Hou, P., Zhao, G., He, C., Wang, H. & He, H. Biopanning of polypeptides binding to bovine ephemeral fever virus G(1) protein from phage display peptide library. *BMC Vet. Res.* **14**, 3 (2018).
55. Lv, L., Zhao, G., Wang, H. & He, H. Cholesterol 25-Hydroxylase inhibits bovine parainfluenza virus type 3 replication through enzyme activity-dependent and -independent ways. *Vet. Microbiol.* **239**, 108456 (2019).
56. Chen, S. et al. Epithelial PBLD attenuates intestinal inflammatory response and improves intestinal barrier function by inhibiting NF-kappaB signaling. *Cell Death Dis.* **12**, 563 (2021).
57. Hou, P. et al. The ORF7a protein of SARS-CoV-2 initiates autophagy and limits autophagosome-lysosome fusion via degradation of SNAP29 to promote virus replication. *Autophagy* **19**, 551–569 (2023).
58. Hsu, W. L., Saffran, H. A. & Smiley, J. R. Herpes simplex virus infection stabilizes cellular IEX-1 mRNA. *J. Virol.* **79**, 4090–4098 (2005).
59. Wang, X. et al. Sindbis virus can exploit a host antiviral protein to evade immune surveillance. *J. Virol.* **90**, 10247–10258 (2016).
60. Eberhardt, J., Santos-Martins, D., Tillack, A. F. & Forli, S. AutoDock vina 1.2.0: new docking methods, expanded force field, and python bindings. *J. Chem. Inf. Model.* **61**, 3891–3898 (2021).
61. Zhou, Y. et al. Gastrodin inhibits virus infection by promoting the production of type I interferon. *Front. Pharmacol.* **11**, 608707 (2020).

Acknowledgements

The study was partially supported by grants from the National Natural Science Fund of China (32373000 to P.H.; 32072834 to H.H.), Shandong Provincial Natural Science Foundation, China (ZR2021MC050 to P.H.; ZR202212030212 to X.L.), Jinan Innovation Team (202228060 to H.H.), Jinan Research Pioneer Workshop (202333059 to H.W.).

Author contributions

H.H. and H.W. developed the concept of the study; H.H. and P.H. designed the experiments; H.Z., Y.G., Y.L., and F.Z. performed the experiments; X.L., Y.G., and X.S. participated in the viral infection experiments; J.W., X.Y.W., Y.F., and X.M.W. helped construct the recombinant plasmids. F.C., H.Z., and Y.G. performed the mouse experiments; X.L., F.C., Y.G., and H.Z. collected and analyzed the data; P.L.H. wrote the manuscript; D.C.H. made revisions to the writing. H.W.

and H.H. supervised the study. All the authors read and approved the final manuscript.

Competing interests
The authors declare no competing interests.

Additional information
Supplementary information The online version contains supplementary material available at https://doi.org/10.1038/s41467-024-54882-y.

Correspondence and requests for materials should be addressed to Hongmei Wang or Hongbin He.

Peer review information *Nature Communications* thanks the anonymous reviewers for their contribution to the peer review of this work. A peer review file is available.